Utrecht University

The Mid-Pleistocene Transition: a dynamical systems approach

Master thesis for the study programmes
Meteorology, Physical Oceanography and Climate
and
Mathematical Sciences
at Utrecht University

Author information:

Felix E. Nolet

Mathematical Institute, Utrecht University
&
Institute for Marine and Atmospheric Research, Utrecht University

Supervisors:

dr. Anna S. von der Heydt
Institute for Marine and Atmospheric Research, Utrecht University

prof. dr. Sjoerd M. Verduyn Lunel
Mathematical Institute, Utrecht University

Abstract

In this project, we investigated the Mid-Pleistocene transition (the change of glacial period from 41 kyr to 100 kyr, around 800 kyr ago), with a dynamical systems approach. By first introducing the mathematical structure for such transitions in systems (dynamical systems, bifurcations and tipping), this can use this theory to find 100 kyr cycles in dynamical systems and simulate transitions such as the Mid-Pleistocene transition (MPT). This is first investigated in the conceptual climate model of Saltzman and Maasch [1]. By first studying a simplified version of this model, a thorough bifurcation analysis is performed. By knowing more about the dynamics of the model, it is possible to simulate the MPT in this model by crossing a Hopf bifurcation. Although this does not give a proof of a physical mechanism that triggers the MPT, it seems that MPT-like transitions are (in these systems) triggered by parameter(s) in the CO_2 equations. Later on, also MPT-like transitions are simulated in the more physics-based model of Gildor and Tziperman [2, 3]. In this model, only a small change in parameters (seemingly without crossing a bifurcation) is enough to simulate MPT behavior.

Contents

Introduction

The climate on earth is not constant, as we of course observe with global warming. However, also on timescales of tens of thousands of years, climate is variable. Approximately every 100000 years (100 kyrs) we have an ice age, i.e. a period with lower surface and atmosphere temperatures, with the presence of extensive ice sheets at the poles. In between two ice ages, we have a warmer period on earth. In glaciology, the cold and warm periods are often referred to as glacials and interglacials. In the sense of the presence of ice sheets on the north and south pole, we are also currently in an ice age.

Naturally, the question arises how we know this period of ice ages. For this we need measurements of ice volume and temperature on earth over very long periods of time (at least a multiple of the period of 100 kyr). There are of course no direct measurements of temperature and ice volume of the last few million years. For that reason, we have to use indirect data, which are mainly from isotope measurements from icecores and deep sea cores. Often used for this reconstruction, is the $\delta^{18}\mathrm{O}$ value, defined as

$$\delta^{18}\mathrm{O} = \frac{R_{\text{sample}}}{R_{\text{standard}}} - 1 \qquad \text{where } R = \frac{\text{mass } \mathrm{H_2^{18}O}}{\text{mass } \mathrm{H_2O}} \tag{1}$$

which is sometimes multiplied by 1000‰. This number gives the ratio of stable isotopes $^{18}\mathrm{O}$ and $^{16}\mathrm{O}$, which for example in deep sea cores depends on the ratio in the surrounding ocean water. The $\delta^{18}\mathrm{O}$ value on the long term (many years) is believed to be correlated to the global temperature. Since the $^{18}\mathrm{O}$ isotope is slightly heavier than the $^{16}\mathrm{O}$ isotope, it is less likely to evaporate. This means that in clouds, there is less $^{18}\mathrm{O}$ than in the oceans. Since ice sheets (on land) are formed from snow, one would expect also lower $\delta^{18}\mathrm{O}$ values there, compared to the ocean. As global temperatures decrease, more water is stored in the ice sheets, increasing the $\delta^{18}\mathrm{O}$ value of the oceans. A linear approximation gives an estimate of 0.22‰ increase in $\delta^{18}\mathrm{O}$ per 1 K temperature decrease. A quadratic extrapolation gives the relation

$$T = 16.5 - 4.3\delta + 0.14\delta^2 \tag{2}$$

with T in °C and δ denoting the $\delta^{18}\mathrm{O}$ value [4]. For the deep sea cores, expect of temperature T also ice volume V is believed to be a driver of $\delta^{18}\mathrm{O}$. A first order approximation is given by

$$\delta^{18}\mathrm{O} \approx a + bT + cV \tag{3}$$

with constants $a, b, c \in \mathbb{R}$. Literature on isotope measurements suggests values of $a = 0.00263 \equiv 2.63‰$, $b = -0.00025\ \mathrm{K^{-1}} \equiv -0.25‰\ \mathrm{K^{-1}}$ and $c = 0.4 \cdot 10^{-19}\ \mathrm{m^{-3}} \equiv 0.4 \cdot 10^{-16}‰\ \mathrm{m^{-3}}$ [5]. Since $b < 0$, we see that temperature increases with decreasing values of $\delta^{18}\mathrm{O}$. For ice cores, b and c change sign, so temperature increases with increasing $\delta^{18}\mathrm{O}$.

In figure 1 a δ^{18}O record is presented until to 1.5 Myr ago. We observe that until 800 kyr ago, the periodicity was about 40 kyr, instead of the 100 kyr period we have since. This means also that ice ages were more frequent than they are now. The sudden change or transition in this periodicity, is referred to as the 'Mid-Pleistocene transition' (since the Pleistocene is the period from about 2.6 million years to 11700 years ago).

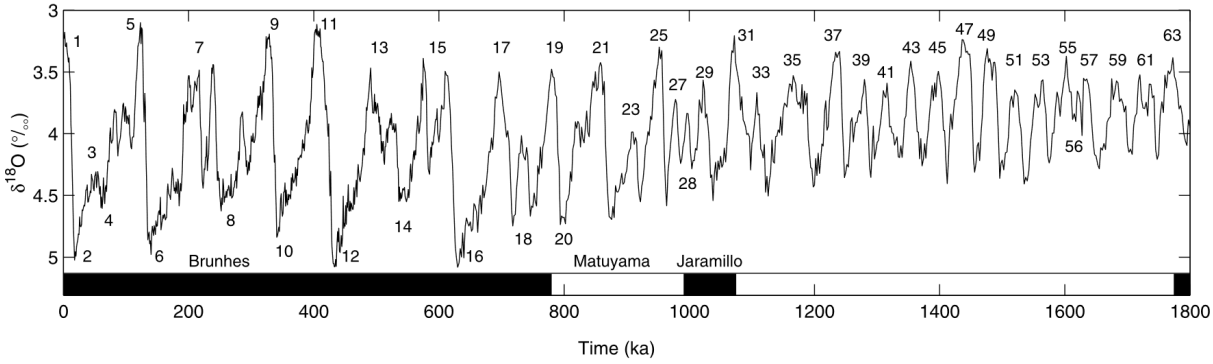

Figure 1: δ^{18}O measurements until 1.5 Myr ago. Time from right to left. Figure from [6].

But what drives the climate such that we observe these cycles? On these time scales, our earth's climate is driven by the energy input of the sun (i.e. the *insolation*). This insolation varies in time and depends on different periodicities in the position and orbit of the earth relative to the sun. Examples are the axial tilt of the earth, the eccentricity of the orbit of the earth around the sun and the precession of this orbit. These forcings have different periods, and are often called the *Milankovitch cycles*. Different cycles are shown in figure 2.

If the insolation, driven by these Milankovitch cycles, determines the climate on earth (and therefore glacials and interglacials), does it then also explain the Mid-Pleistocene transition (MPT)? This question is not easy to answer. Since the Milankovitch cycles themselves have been the same for a very long time (they do not change qualitatively 800 kyr ago), it is unlikely that they triggered the MPT. In figure 2, we see that there is a periodicity of 41 kyr (tilt) in the signal, which could force the earth's climate to the same periodicity. In that sense, we can 'explain' the periodicity before the MPT. There is also a Milankovitch cycle of 96 kr (eccentricity), which is not exactly the same as the periodicity of the δ^{18}O levels after the MPT, but it is close. However, one should note that this cycle is a lot weaker than the one forced by the axial tilt (41 kyr). The most energy of the spectrum of the insolation is at the period of the tilt/obliquity (41 kyr), followed by the precession (21 and 23 kyr). Only a very small amount of the energy can be found at the period of eccentricity, making it very unlikely that it can trigger such large amplitude ice ages. Therefore, it has remained unclear what triggered the transition to a periodicity of 100 kyr.

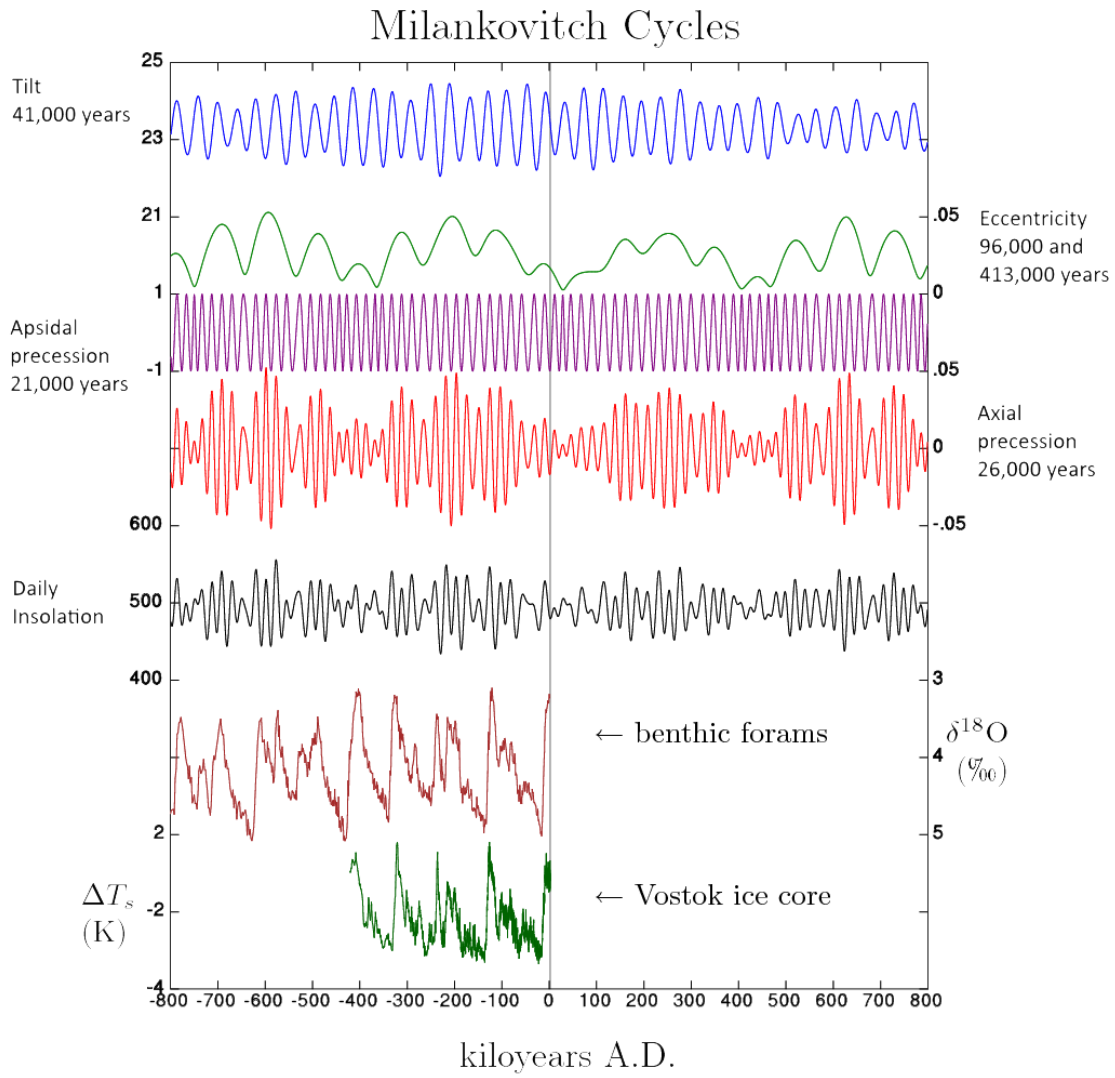

Figure 2: Milankovitch cycles and $\delta^{18}O$ measurements. Upper four graphs (colored) are different Milankovitch cycles, the fifth graph (insolation, summer solstice at 65°N) is a combination of those, giving the input for the climate. The last two curves are from $\delta^{18}O$ measurements from benthic and ice cores, with data of [6] and [7].

For a long time this so-called "100 kyr problem" has been investigated by the scientific community, however, there still is not a universal answer. However, there are quite some different explanations in attempt to solve this problem. We will discuss two classes of theories, that are the most common.
In the first class of theories, it is believed that the 100 kyr period is an internal period of the climate. Theories are different in the process that triggered the MPT, but the general idea is the same. The idea is that the 100 kyr frequency is the earth's natural resonance frequency, caused by feedback processes within the climate system. This resonance should

then have been developed or intensified at the MPT, in order to trigger the transition. Otherwise the 100 kyr periodicity should also have been present before 1 Myr ago. A slow parameter change is an example of such a trigger [8, 2]. An example of a parameter that could have triggered the transition is the deep sea temperature [9]. Another example, is the theory of Clark et al., suggesting that a transition of the Laurentide ice sheet (from soft bedded to mixed hard-soft bedded) can also trigger the MPT [10].
In the second class of theories, the external forcing (insolation), and the earth's response to this, is the leading factor in explaining the MPT. An example of that is the theory of the 'skipped obliquity'. It assumes that obliquity (axial tilt) is the leading driver (as is the case in the theory of Milankovitch). Due to interactions and feedbacks, the pacing of the climate system is not one-to-one with the obliquity of 41 kyr, leading to skipping of cycles. This can double (or triple) the period in the temperature record, leading to 82 and 123 kyr periods [11]. Another example is the theory of fluctuations in the solar luminosity. The earth's climate can respond to diffusion waves in the sun and a climate transition could then be triggered, such as the MPT [12]. However, there are also measurements (for example Helium isotope measurements) that contradict this theory [13].
There are even more theories, so it remains an understatement that the scientific community is still investigating the MPT and is that there is not one overall theory to solve this problem. Investigating the MPT is important, not only for trying to solve the 100 kyr problem itself, but it can give an insight in our climate system and its response to the external forcing by the sun. Knowing more about past climate shifts or transitions, and the triggers of such transitions, could give indications for future climate change as well. It gives a deeper understanding of our climate system and interacting components.

In this project we will use the theory of dynamical systems and bifurcations, in attempt to explain in both a mathematical and a physical sense this transition in periodicity in the climate system. We believe that a transition as the MPT can be seen as a so-called *tipping point* in a dynamical system. There are multiple types of tipping points, we will focus on those that are triggered by bifurcations.
In the first chapter, we will give a mathematical background, discussing dynamical systems, bifurcation theory and we will define the notion of tipping points. In the second chapter, the theory is applied to a simple conceptual climate model in attempt to simulate tipping points that have the same character as the MPT, and investigate which features in the dynamical system can trigger these tipping points. Lastly, in chapter 3 a larger (and more realistic) physics-based climate model is studied, to see whether the periodicity transition behaviour persists when the dimension is increased.

1 Mathematical background

In this section, we will at first give the mathematical setting and introduce the theory of dynamical systems. Secondly, an overview of bifurcation theory is given, to define some of the terminology that is used further on in this thesis. Lastly, we will explain how we can simulate transitions (such as the MPT) by introducing time dependence.

Notation for the reader: statements (such as definitions, examples, lemmas and theorems) are ended with a $\triangle$, remarks are ended with $\diamondsuit$ and proofs are ended with $\square$.

1.1 Introduction to dynamical systems

1.1.1 Definition of a dynamical system

In this project, we work in the world of continuous-time dynamical systems, described by ordinary differential equations (ODEs). If we have n coordinates (or variables, state vectors, ...), our state space (also called phase space) is $\mathbb{R}^n$ and a dynamical system is described by n ODEs. In vector form, a dynamical system will look like

$$\frac{dx}{dt} = f(x) \tag{4}$$

for our state vector $x = (x_1, x_2, ..., x_n) \in \mathbb{R}^n$. The function $f : \mathbb{R}^n \to \mathbb{R}^n$ described the evolution in time of the variables, and is assumed to be smooth (sufficiently many times differentiable). Often the dot-notation is used for the time derivative, i.e. the equation

$$\dot{x} = f(x) \tag{5}$$

is equivalent to equation (4). The ODEs are called *autonomous*, meaning that the function f does not depend on time, only on the position in state space.

Remark. With using the term smooth, we implicitly also assume the function to be locally Lipschitz continuous. In that case, there is exists a (local) unique solution of 5 for given initial condition $x(t_0) = x_0$. [14] $\diamondsuit$

Often rather simple is the class of linear dynamical systems. In that case we can write the right hand side of equation (4) as a matrix multiplication.

Definition 1.1. A dynamical system on (a subset of) $\mathbb{R}^n$ is called linear if there exists a real-valued $n \times n$ matrix $\mathbf{A}$ such that

$$\frac{dx}{dt} = \mathbf{A}x. \tag{6}$$

$\triangle$

Recall that a higher order ODE can be written as a set of ODEs. We illustrate this with the following example.

Example 1.1. Given some $\omega \in \mathbb{R}$ and the second order differential equation

$$\ddot{x} = -\omega^2 x \tag{7}$$

we can, introducing $y = \dot{x}$, write this as the two ODEs

$$\frac{d}{dt}\begin{pmatrix} x \\ y \end{pmatrix} = \begin{pmatrix} y \\ -\omega^2 x \end{pmatrix} = \begin{pmatrix} 0 & 1 \\ -\omega^2 & 0 \end{pmatrix}\begin{pmatrix} x \\ y \end{pmatrix} \tag{8}$$

which is in fact a linear dynamical system on $\mathbb{R}^2$. Thus a higher order derivative does not imply nonlinearity of the equivalent dynamical system. △

Remark. The ODE in example 1.1 is that of a harmonic oscillator with frequency $\omega \in \mathbb{R}$, which has solutions of the form

$$x(t) = A\cos(\omega t) + B\sin(\omega t) \tag{9}$$

with $A, B \in \mathbb{R}$ depending on initial conditions. ♢

Although we speak of *solutions*, we mean of the corresponding ODE (for which existence of solutions is defined). However, often one speaks of *orbits* of the dynamical system. We will define what is meant by this.

Definition 1.2. Let $x_0 \in \mathbb{R}^n$ and let $I \subset \mathbb{R}$ be a time interval where the dynamical system as in equation (4) or (5) has a solution $x(t; x_0)$ for initial condition x_0. Then the corresponding *orbit* is a curve in state space, given by

$$\mathcal{O}(x_0) = \{x \in \mathbb{R}^n \mid \exists\, t \in I : x = x(t; x_0)\}\,. \tag{10}$$

△

Remark. Note that different points in phase space can be on the same orbit. An orbit also has a *direction* or *orientation*. This direction is always towards increasing t. ♢

Definition 1.3. A *phase portrait* of a dynamical system is the collection of all its distinct orbits. △

Remark. For practical and graphical reasons, when drawing a phase portrait only some of the orbits are drawn. The rest then follows from continuity. ♢

The operator that maps to a point on the orbit at a time t, is called the *flow* operator or *evolution* operator (given an initial condition). We define this more precisely.

Definition 1.4. Let $x_0 \in \mathbb{R}^n$ be an initial condition for system (4). Then the flow $\varphi^t : \mathbb{R}^n \to \mathbb{R}^n$ maps this point to a point on its orbit, t time units later, i.e.

$$\varphi^t x_0 = x(t; x_0). \tag{11}$$

△

1.1.2 Equilibria

As is known, not all differential equations have solutions, or at least we cannot always find them. Still we want to say something about the behaviour of a dynamical system as in equation (4). The first thing one does, is look for equilibria of the system. These are stationary points in state space (i.e. taking such a point as initial condition will give a constant solution).

Definition 1.5. A point $x_0 \in \mathbb{R}^n$ is called an *equilibrium* of system (4) if $f(x_0) = 0$. $\triangle$

Remark. The orbit of an equilibrium consists only of one point, that of the equilibrium itself. Thus $\mathcal{O}(x_0) = \{x_0\}$. $\diamondsuit$

Lemma 1.1. *If $x_0 \in \mathbb{R}^n$ is an equilibrium of (4), then $\varphi^t x_0 = x_0$ for all $t \in \mathbb{R}$.* $\triangle$

Remark. Sometimes this is used as the definition of an equilibrium, and then $f(x_0) = 0$ follows from that. The two statements are equivalent. $\diamondsuit$

We will introduce the notion of stability of such an equilibrium. In this way, something can be said about the behaviour of the system close to this equilibrium. We will call an equilibrium *stable* when orbits close to it, will converge towards the equilibrium (and *unstable* otherwise). From the Hartman-Grobman theorem (which we will not repeat), we know that the linearization of the system around an equilibrium determines the stability. We repeat the theorem of Lyapunov (1892) from [15].

Theorem 1.2. *Suppose that $x_0 \in \mathbb{R}^n$ is an equilibrium of the system as in (4). Let $\mathbf{A} = Df(x_0)$ denote the Jacobian matrix of f evaluated at the equilibrium. Then x_0 is* stable *if all eigenvalues $\lambda_1, ..., \lambda_n$ of $\mathbf{A}$ satisfy* $\mathrm{Re}(\lambda) < 0$. $\triangle$

As soon as there is one eigenvalue that has $\mathrm{Re}(\lambda) > 0$, the system is unstable. Sometimes a system with all eigenvalues $\mathrm{Re}(\lambda) \leq 0$ and at least one with $\mathrm{Re}(\lambda) = 0$, is called neutrally stable. In this case, the dynamics can be more complicated than when there are no eigenvalues on the imaginary axis.

Definition 1.6. An equilibrium $x_0 \in \mathbb{R}^n$ of (4) is called *hyperbolic* if all eigenvalues of the Jacobian matrix of f at x_0 have $\mathrm{Re}(\lambda) \neq 0$. $\triangle$

Example 1.2. Let $\alpha, \beta > 0$. Consider the linear dynamical system on $\mathbb{R}^2$, defined by

$$\frac{d}{dt}\begin{pmatrix} x \\ y \end{pmatrix} = \begin{pmatrix} -\alpha x \\ -\beta y \end{pmatrix} = \begin{pmatrix} -\alpha & 0 \\ 0 & -\beta \end{pmatrix}\begin{pmatrix} x \\ y \end{pmatrix} \tag{12}$$

which has an equilibrium at the origin. We can read of the matrix $\mathbf{A}$ immediately. Its eigenvalues are $\lambda_1 = -\alpha$ and $\lambda_2 = -\beta$, so we have $\mathrm{Re}(\lambda) < 0$ for both. Therefore the origin is a *stable* equilibrium and orbits will converge towards the origin. A phase portrait is plotted in figure 3 for fixed α and β. $\triangle$

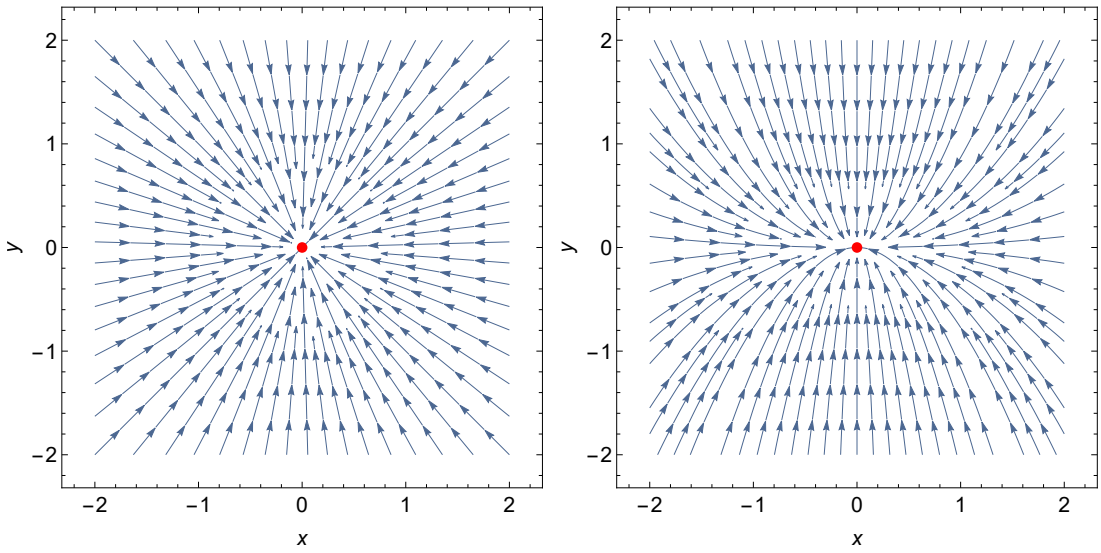

Figure 3: Phase portrait for system (12) with $(\alpha, \beta) = (1, 1)$ (left) and $(\alpha, \beta) = (1, 2)$ (right). In red the (stable) equilibrium at the origin.

Note that although different values for β are used, the two phase portraits look qualitatively the same. This can be generalized for any two dynamical systems with an equilibrium.

Definition 1.7. Let $f, g : \mathbb{R}^n \to \mathbb{R}^n$ be smooth functions. Let $\dot{x} = f(x)$ and $\dot{y} = g(y)$ be two dynamical systems on $\mathbb{R}^n$ with equilibria at x_0 and y_0, respectively. We call the dynamical systems *topologically equivalent* near their equilibria if there exists a homeomorphism $h : \mathbb{R}^n \to \mathbb{R}^n$ that satisfies the following conditions:

1. h is defined in a neighborhood $U \subset \mathbb{R}^n$ of x_0.
2. h satisfies $h(x_0) = y_0$.
3. h maps orbits onto orbits, preserving direction.

△

If the equilibria x_0 and y_0 as in definition 1.7 are hyperbolic, the eigenvalues of the Jacobian again give the necessary information to determine whether two systems are topologically equivalent. This is stated in the next theorem without proof (for that we refer to [15]).

Theorem 1.3. *Let $f, g : \mathbb{R}^n \to \mathbb{R}^n$ be smooth functions. Let $\dot{x} = f(x)$ and $\dot{y} = g(y)$ be two dynamical systems on $\mathbb{R}^n$ with hyperbolic equilibria at x_0 and y_0, respectively. Suppose the number of the Jacobian matrices at these equilibria have the same number of eigenvalues with $\mathrm{Re}(\lambda) > 0$ and $\mathrm{Re}(\lambda) < 0$, respectively. Then the two systems are topologically equivalent.* △

As is shown, one could already extract some information of the dynamics of the system, by determining the equilibria (which is simply finding zeros of a function) and calculation the eigenvalues of the Jabocian matrix at these points. This is therefore always a good starting point when investigating a dynamical system.

1.1.3 Periodic orbits

As we have seen in the previous paragraph, equilibria are points that are *invariant* under the flow, i.e. $\varphi^t x_0 = x_0$ for all $t \in \mathbb{R}$, if x_0 is an equilibrium. In other words, the orbit of x_0 (which only consists of the point itself) maps to itself under φ. This might also be the case for other orbits, that contain more than one point.
Let $\mathcal{C}$ be a closed curve in state space ($\mathbb{R}^n$). Suppose this curve is an orbit of the dynamical system as in (4), i.e. $\mathcal{C} = \mathcal{O}(x)$ for all $x \in \mathcal{C}$. Then we call C a periodic orbit or *cycle* of the system. This can also be defined using the flow.

Definition 1.8. An orbit $\mathcal{C}$ of a dynamical system is called a *cycle* if it is not an equilibrium and there exists $T > 0$ such that every $x \in \mathcal{C}$ satisfies $\varphi^{t+T} x = \varphi^t x$ for every $t \in \mathbb{R}$. △

Similarly as in the case of equilibria, we want to know if a cycle is stable, i.e. if orbits close to this curve will converge towards the cycle or diverge. For that, we need the notion of a Poincaré map. Let x_0 be a point on the cycle $\mathcal{C}$. Then we define Σ as cross-section, which is a hypersurface of dimension $n - 1$. For $x \in \Sigma$, the Poincaré map P is defined as the point on Σ where the orbit of x returns 'after one rotation' (if it exists). This is illustrated in figure 4.

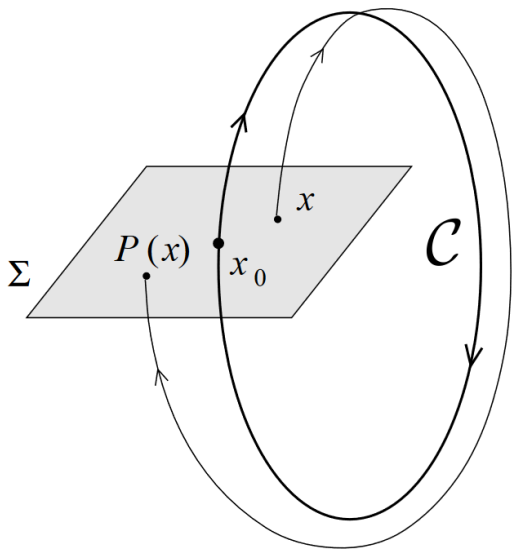

Figure 4: Illustration of a Poincaré map. Adapted figure from [15].

Note that for the point x_0 we have $P(x_0) = x_0$, i.e. it is a fixed point of the Poincaré map. In general, one can find cycles by solving for fixed points of a Poincaré map. If we now take a point $x \in \Sigma$ close to x_0, we want to know if the iterations of x under P are getting closer to x_0. In that case, the orbits close to the cycle will converge towards the cycle (which makes it a stable cycle). Similarly as for the equilibria, we look at the Jacobian matrix of P at x_0. With the eigenvalues of this matrix, we have similar notions of hyperbolicity and stability.

Definition 1.9. The cycle $\mathcal{C}$ is called *hyperbolic* if all eigenvalues $\mu_1, ..., \mu_{n-1}$ of the Poincaré map at x_0, are not located at the unit circle, i.e. $|\mu| \neq 1$. △

Definition 1.10. The cycle $\mathcal{C}$ is called *stable* if all eigenvalues $\mu_1, ..., \mu_{n-1}$ of the Poincaré map at x_0 satisfy $|\mu| < 1$. △

Remark. The eigenvalues $\mu_1, ..., \mu_{n-1}$ are also called *multipliers* and are independent of the point x_0 on the cycle. ♢

We now have an idea of some of the dynamics of a dynamical system without solving any differential equation. The equilibria and cycles already give us some information. Of course there may also be other subsets $\mathcal{S} \subset \mathbb{R}^n$ of state space that are invariant, but are not equilibria or cycles. The definition of being invariant, is therefore more general.

Definition 1.11. A subset $\mathcal{S} \subset \mathbb{R}^n$ is called an *invariant set* of a dynamical system, if for every $x \in \mathcal{S}$ is mapped onto $\mathcal{S}$ under the flow, i.e. $\varphi^t x \in \mathcal{S}$ for all $t \in \mathbb{R}$. △

Remark. Every individual orbit is an invariant set. ♢

One could always restrict the dynamical system to an invariant subset $\mathcal{S}$ (instead of the whole phase space). This is again a dynamical system, with restricted flow $\varphi^t|_{\mathcal{S}} : \mathcal{S} \to \mathcal{S}$.

1.2 Bifurcation theory

1.2.1 Introduction

In general, bifurcation theory is the mathematical theory that describes changes in the topological structure of a given family. In our case, we will investigate families of dynamical systems and study changes in the topological structure. So far, we studied properties of dynamical systems and defined topological equivalence of two systems. In the setting of bifurcation theory, we study families of such dynamical systems. To make this more explicit, we will introduce an explicit dependence on parameters in the system. In this setting, every dynamical system is of the form

$$\dot{x} = f(x, \alpha) \tag{13}$$

where again $x \in \mathbb{R}^n$ is the state vector. $\alpha \in \mathbb{R}^s$ is the parameter and we again assume that the function $f : \mathbb{R}^n \times \mathbb{R}^s \to \mathbb{R}^n$ is smooth. For any fixed parameter α, we are back in the setting of equation (4) and (5). When α is changed, the phase portrait of the system

also changes. Depending on this change, the new phase portrait could be topologically equivalent to the old one. However, this does not have to be the case. This is how we will define a bifurcation.

Definition 1.12. A *bifurcation* is the appearance of a topologically nonequivalent dynamical system, under variation of α. △

One possibility of a bifurcation is that the number of equilibria changes for changing α. Then the new system is topologically nonequivalent. Also a cycle might appear, or the number of cycles can change. Or the stability of an equilibrium or cycle can change, also leading to a bifurcation.
We will investigate some of the 'standard' bifurcations that one could expect in a family of dynamical systems. The first type of bifurcations are the bifurcations of equilibria. After that, we will also shortly discuss some bifurcations of periodic orbits.

1.2.2 Codim 1 bifurcations of equilibria

In this paragraph we will study some bifurcations of codimension 1, meaning that one parameter is sufficient to encounter these bifurcations. Therefore, our dynamical system is now given by

$$\dot{x} = f(x, \alpha); \qquad x \in \mathbb{R}^n,\ \alpha \in \mathbb{R} \tag{14}$$

which corresponds to $s = 1$ in the previously defined system. Suppose that the system has an hyperbolic equilibrium at $x_0 \in \mathbb{R}^n$, for some $\alpha_0 \in \mathbb{R}$. This means that all eigenvalues have $\mathrm{Re}(\lambda) \neq 0$. When we change the parameter α, also the eigenvalues change. If this change is small enough, the equilibrium will still be hyperbolic, with the name number of eigenvalues left (stable) and right (unstable) to the imaginary axis. In that case, the new system is then topologically equivalent to the system at α_0. However, it can happen that the equilibrium is not hyperbolic anymore (one or more eigenvalues hit the imaginary axis) and with even larger change of α the number of stable and unstable eigenvalues might change, leading to a topologically nonequivalent system (i.e. a bifurcation occurs).

Remark. In systems including parameters (such as above), we also speak about eigenvalues. To be precise, these are the eigenvalues of the Jacobian matrix of the function f with respect to the state vector x (evaluated at the equilibrium), i.e. eigenvalues of the $n \times n$ matrix $D_x f(x_0, \alpha)$. ♢

There are different possibilities of eigenvalue(s) that hit the imaginary axis when α changes. These lead to different kind of bifurcations, we will discuss a few of them.

Definition 1.13. Suppose for one eigenvalue λ_j ($j \in \{1, ..., n\}$) we get $\lambda_j = 0$ at some parameter value α. This is called a *fold* bifurcation. △

Remark. Other names for fold bifurcation are *saddle-node* bifurcation or *limit point* bifurcation. ♢

Definition 1.14. Suppose that at some parameter value α, a pair of complex conjugate eigenvalues hit the imaginary axis, i.e. $\lambda_{1,2} = \pm i\omega$ for some $\omega > 0$, where λ_1, λ_2 are two of the eigenvalues. This is called an *Andronov-Hopf* bifurcation (often called *Hopf*). $\triangle$

Remark. Note that a fold bifurcation can already occur in one-dimensional systems ($n = 1$), but an Andronov-Hopf bifurcation can only occur when the dimension is $n \geq 2$. $\diamondsuit$

Example 1.3. We will investigate bifurcations of the set of two ODEs,

$$\begin{cases} \dot{x}_1 &= \alpha - x_1^2 \\ \dot{x}_2 &= -x_2 \end{cases} \tag{15}$$

with parameter $\alpha \in \mathbb{R}$. Using $x = (x_1, x_2) \in \mathbb{R}^2$, we write this as one dynamical system

$$\dot{x} = f(x, \alpha) \equiv \begin{pmatrix} \alpha - x_1^2 \\ -x_2 \end{pmatrix} \tag{16}$$

and we find the Jacobian matrix of f w.r.t. x to be

$$D_x f(x, \alpha) = \begin{pmatrix} -2x_1 & 0 \\ 0 & -1 \end{pmatrix}. \tag{17}$$

To find equilibria of the system, we solve $f(x_0, \alpha) = 0$ and find $x_0 = (\pm\sqrt{\alpha}, 0)$. Note that this is only valid for $\alpha \geq 0$, otherwise there are no solutions (and thus no equilibria). For positive α, we find one positive and one negative equilibrium (w.r.t to the first coordinate). We call the Jacobian matrices evaluated at these equilibria $\mathbf{A}_+$ and $\mathbf{A}_-$, respectively. We can calculate these matrices:

$$\mathbf{A}_+ = \begin{pmatrix} -2\sqrt{\alpha} & 0 \\ 0 & -1 \end{pmatrix}, \qquad \mathbf{A}_- = \begin{pmatrix} 2\sqrt{\alpha} & 0 \\ 0 & -1 \end{pmatrix}. \tag{18}$$

The eigenvalues of the matrices determine the stability of the corresponding equilibrium. Since the eigenvalues are in this case equal to the two nonzero entries, we see that the positive equilibrium is stable and the negative equilibrium unstable. At $\alpha = 0$, one of the eigenvalues becomes zero, i.e. here we find a fold bifurcation. Phase portraits for values of $\alpha = 0$ and close to this, are drawn in figure 5. We see that when α becomes negative (i.e. when we cross the bifurcation at $\alpha = 0$), two equilibria have merged into one, and disappeared. This becomes clear when we plot the first coordinate of the equilibrium position as function of α, as can be seen in figure 6. $\triangle$

In example 1.3, we have seen a 2-dimensional dynamical system with a fold bifurcation. In general, if we have such a system, we do not want to calculate and draw everything to find this bifurcation. Luckily, there is a shorter solution to this, as we see in the next theorem.

Theorem 1.4. *Let $\alpha \in \mathbb{R}$ be a parameter of the planar dynamical system*

$$\dot{x} = f(x, \alpha) \tag{19}$$

with an equilibrium at x_0 and let $\mathbf{A}$ denote the Jacobian matrix $D_x f$ at x_0. If at some $\alpha_0 \in \mathbb{R}$ we have $\det(\mathbf{A}) = 0$ and $\mathrm{tr}(\mathbf{A}) \neq 0$, then there is a fold bifurcation at α_0. $\triangle$

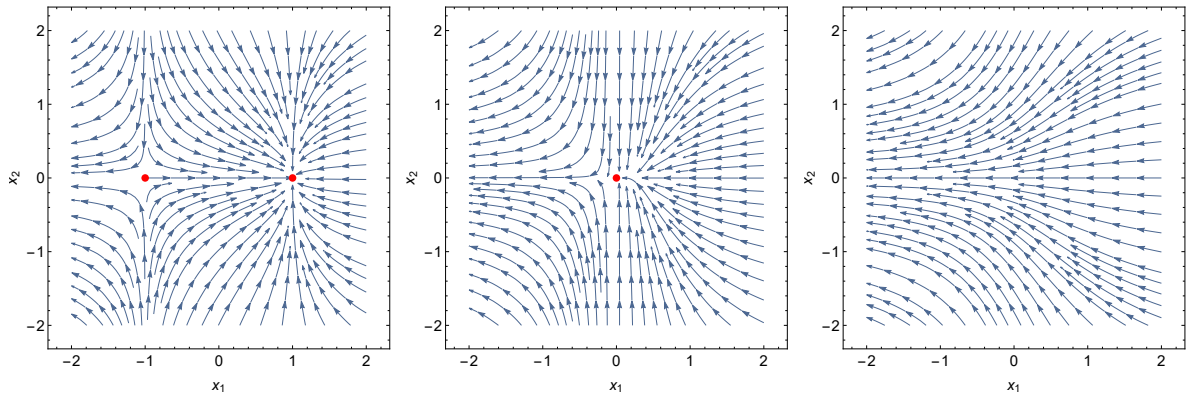

Figure 5: Phase portraits for system (16) for $\alpha = 1$ (left), $\alpha = 0$ (middle) and $\alpha = -1$ (right). Red dots indicate equilibria.

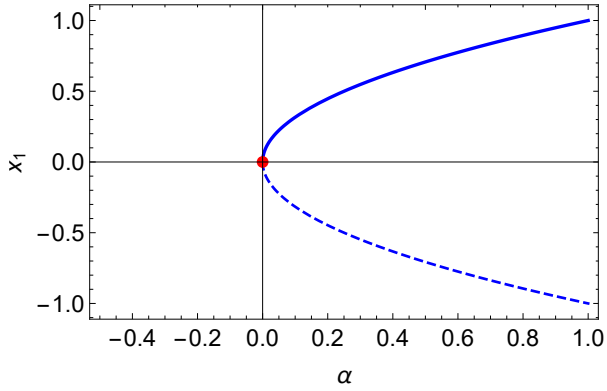

Figure 6: First coordinate of the equilibrium position as function of α. Solid line indicates a stable equilibrium, dashed is unstable. At $\alpha = 0$, the two equilibria merge (red dot).

Proof. The system will have a fold bifurcation if one of the eigenvalues of $\mathbf{A}$ becomes zero. In general, we can write

$$\mathbf{A} = \begin{pmatrix} a_{11} & a_{12} \\ a_{21} & a_{22} \end{pmatrix} \tag{20}$$

of which we can find the eigenvalues by solving the characteristic equation,

$$(a_{11} - \lambda)(a_{22} - \lambda) - a_{12}a_{21} = 0 \tag{21}$$

which is equivalent to solving

$$\lambda^2 - \mathrm{tr}(\mathbf{A})\lambda + \det(\mathbf{A}) = 0 \tag{22}$$

where $\mathrm{tr}(\mathbf{A}) = a_{11} + a_{22}$ and $\det(\mathbf{A}) = a_{11}a_{22} - a_{12}a_{21}$. The solutions $\lambda_{1,2}$ are

$$\lambda_{1,2} = \frac{\mathrm{tr}(\mathbf{A}) \pm \sqrt{\mathrm{tr}(\mathbf{A})^2 - 4\det(\mathbf{A})}}{2} \tag{23}$$

and if $\det(\mathbf{A}) = 0$ and $\mathrm{tr}(\mathbf{A}) \neq 0$, we indeed find

$$\lambda_1 = 0, \qquad \lambda_2 = \pm \mathrm{tr}(\mathbf{A}) \neq 0 \tag{24}$$

which implies a fold bifurcation. □

In this way, we can detect fold bifurcations, by calculating the trace of the matrix. Especially when doing this numerically, this can be a lot faster than calculating eigenvalues of a matrix.

Example 1.4. Given the planar dynamical system

$$\begin{cases} \dot{x} &= \alpha x - y - x(x^2 + y^2) \\ \dot{y} &= x + \alpha y - y(x^2 + y^2) \end{cases} \tag{25}$$

with parameter $\alpha \in \mathbb{R}$, we will investigate its bifurcations. The system has an equilibrium at $(0, 0)$. The Jacobian matrix J as function of x and y is given by

$$J(x, y) = \begin{pmatrix} \alpha - 3x^2 - y^2 & -1 - 2xy \\ 1 - 2xy & \alpha - x^2 - 3y^2 \end{pmatrix} \tag{26}$$

which at the equilibrium becomes

$$J(0, 0) = \begin{pmatrix} \alpha & -1 \\ 1 & \alpha \end{pmatrix} \tag{27}$$

with eigenvalues $\lambda_{i,j} = \alpha \pm \sqrt{\alpha^2 - \alpha - 1}$ for some i, . At $\alpha = 0$, the eigenvalues become the complex pair $\lambda_{1,2} = \pm i$, which implies a Hopf bifurcation at this point. In figure 7, we plotted phase portraits of the system around this bifurcation point. When crossing the Hopf bifurcation, the equilibrium becomes unstable and a stable cycle emerges. △

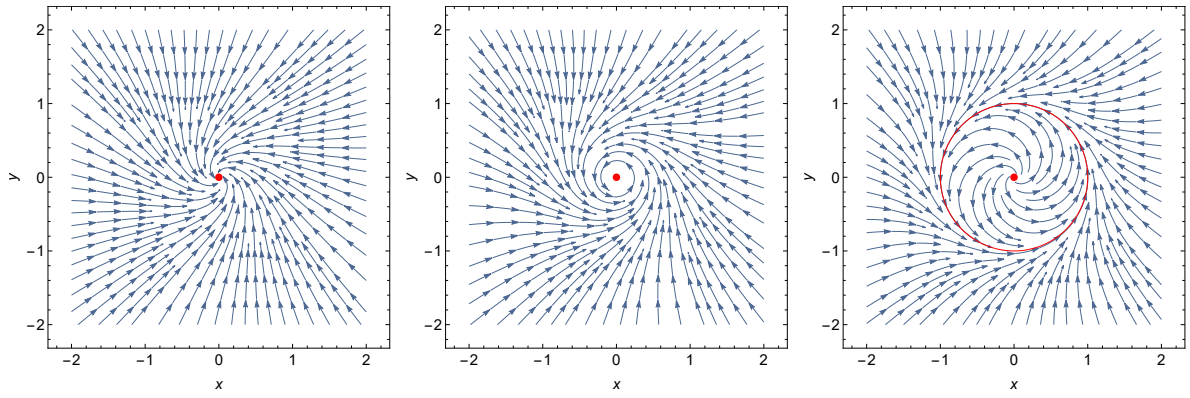

Figure 7: Phase portraits for system (25) for $\alpha = -1$ (left), $\alpha = 0$ (middle) and $\alpha = 1$ (right). Red dots indicate equilibria, the red curve is a cycle.

Example 1.5. We will study a planar dynamical system, very similar to that of example 1.4. The system, with parameter $\alpha \in \mathbb{R}$, is described by the equations

$$\begin{cases} \dot{x} &= -\alpha x - y + x(x^2 + y^2) \\ \dot{y} &= x - \alpha y + y(x^2 + y^2) \end{cases} \tag{28}$$

and it has again an equilibrium at the origin. The Jacobian matrix J at the origin, is now given by

$$J(0,0) = \begin{pmatrix} -\alpha & -1 \\ 1 & -\alpha \end{pmatrix} \tag{29}$$

with eigenvalues $\lambda_{1,2} = -\alpha \pm \sqrt{\alpha^2 - \alpha - 1}$. Again we have $\lambda_{1,2} = \pm i$ at $\alpha = 0$, so an Hopf bifurcation. However, behaviour around this bifurcation is similar as before, but not the same. This can be seen in figure 8, where the phase portraits are shown. We see that in this case, the equilibrium becomes stable and again a cycle emerges. However, this cycle is unstable, since close orbits diverge. △

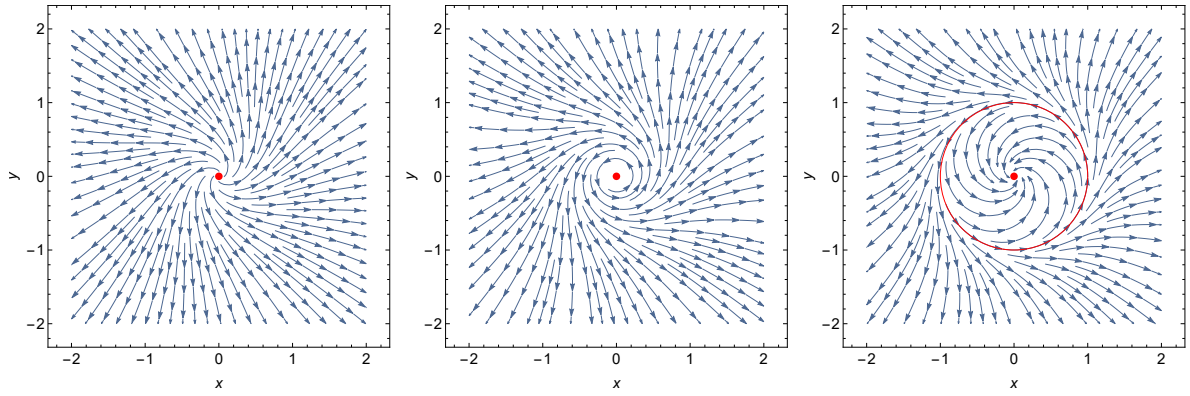

Figure 8: Phase portraits for system (28) for $\alpha = -1$ (left), $\alpha = 0$ (middle) and $\alpha = 1$ (right). Red dots indicate equilibria, the red curve is a cycle.

Remark. In general, crossing a Hopf bifurcation leads to the emergence of a cycle. In the stable case, as in example 1.4, this is called a *supercritical* Hopf bifurcation. The unstable case, as in example 1.5, is called *subcritical*. A proper definition of these types of criticality can be given using the first Lyapunov coefficient l_1, which can be computed when writing out the Taylor series of the function f, for the definition see [15]. The sign of l_1 then determines whether a Hopf bifurcation is supercritical or subcritical. ♢

Theorem 1.5. *Let $\alpha \in \mathbb{R}$ be a parameter of the planar dynamical system*

$$\dot{x} = f(x, \alpha) \tag{30}$$

with an equilibrium at x_0 and let $\mathbf{A}$ denote the Jacobian matrix $D_x f$ at x_0. If at some $\alpha_0 \in \mathbb{R}$ we have $\det(\mathbf{A}) > 0$ and $\mathrm{tr}(\mathbf{A}) = 0$, then there is a fold bifurcation at α_0. △

Proof. Similar as the proof of theorem 1.4, we find the eigenvalues of $\mathbf{A}$ to be

$$\lambda_{1,2} = \frac{\text{tr}(\mathbf{A}) \pm \sqrt{\text{tr}(\mathbf{A})^2 - 4\det(\mathbf{A})}}{2} \tag{31}$$

and when we use the fact that $\det(\mathbf{A}) > 0$ and $\text{tr}(\mathbf{A}) = 0$, we find

$$\lambda_{1,2} = \frac{\pm\sqrt{-4\det(\mathbf{A})}}{2} = \pm\sqrt{\det(\mathbf{A})}i \tag{32}$$

which is a pair of purely imaginary eigenvalues, i.e. there is a Hopf bifurcation. □

Remark. Theorems 1.4 and 1.5 tell us that only by looking at the trace and determinant of the Jacobian matrix, we can detect fold and Hopf bifurcations. This is often much easier to compute than the eigenvalues. ♢

Although there are other codim 1 bifurations of equilibria, we will not further investigate this (since we will not be needing this). We continue with codim 2 bifurcations, which you can encounter by increasing the parameter space with one extra parameter.

1.2.3 Codim 2 bifurcations of equilibria

One could encounter more complicated bifurcations when adding an extra parameter. Just as with the codimension 1 bifurcations, there are also a lot of codim 2 bifurcations. We will discuss two of them, since we will only need these later on in the project. The parameter space becomes two-dimensional, i.e. we study dynamical systems on $\mathbb{R}^n$,

$$\dot{x} = f(x, \alpha) \tag{33}$$

with $\alpha \in \mathbb{R}^2$ and $f : \mathbb{R}^n \times \mathbb{R}^2 \to \mathbb{R}^n$ smooth. We assume that the system has a hyperbolic equilibrium at $x_0 \in \mathbb{R}^n$, for some $\alpha_0 \in \mathbb{R}^2$. When we change α, the eigenvalues of the Jacobian matrix $D_x f(x_0, \alpha)$ change w.r.t. the eigenvalues of $D_x f(x_0, \alpha_0)$. As we saw in the previous paragraph, when one eigenvalue becomes zero, we encounter a fold bifurcation. With the addition of one parameter, more complex (or more degenerate) conditions can be met.

Definition 1.15. Suppose that at some value of α, two of the eigenvalues become $\lambda_1 = \lambda_2 = 0$. This is called a *Bogdanov-Takens* bifurcation. △

Recall that the first Lyapunov coefficient l_1 determines if a Hopf bifurcation is supercritical or subcritical. A special case is when $l_1 = 0$.

Definition 1.16. Suppose that at some value of α, we get $\lambda_{1,2} = \pm\omega i$ for some $\omega > 0$, where λ_1, λ_2 are two of the eigenvalues. Furthermore, suppose that the first Lyapunov coefficient is $l_1 = 0$. This is called a *Bautin* bifurcation. △

Remark. A Bautin bifurcation is also called a *Generalized Hopf* bifurcation. It is a higher degenerate Hopf bifurcation. ♢

Remark. There also exists a higher degenerate fold bifurcation, it is called the *Cusp* bifurcation. It is also a codimension 2 bifurcation.

Example 1.6. Consider the planar dynamical system with parameter $\alpha = (\alpha_1, \alpha_2) \in \mathbb{R}^2$, described by the differential equations

$$\begin{cases} \dot{x} &= y \\ \dot{y} &= \alpha_1 + \alpha_2 x + x^2 - xy \end{cases} \tag{34}$$

and the corresponding Jacobian matrix J is given by

$$J(x, y) = \begin{pmatrix} 0 & 1 \\ \alpha_2 + 2x - y & -x \end{pmatrix}. \tag{35}$$

Note that the system has equilibria at $(\frac{1}{2}(-\alpha_2 \pm \sqrt{\alpha_2^2 - 4\alpha_1}), 0)$. We observe that at $\alpha_1 = \alpha_2 = 0$, the two equilibria have collided to one equilibrium at the origin, and the Jacobian matrix then becomes

$$J(0,0)|_{\alpha=(0,0)} = \begin{pmatrix} 0 & 1 \\ 0 & 0 \end{pmatrix} \tag{36}$$

which has eigenvalues $\lambda_{1,2} = 0$. Therefore, this is a Bogdanov-Takens bifurcation point. We can also find fold and Hopf bifurcations, using theorems 1.4 and 1.5. By looking for zeros of the trace and determinant of the Jacobian matrix, we can find curves in the (α_1, α_2)-plane that correspond to these bifurcations (it will be curves, since the codimension is 1). For the fold bifurcation, we solve $\det(J) = 0$ and find $\alpha_2^2 = 4\alpha_1$. For the Hopf bifurcation, we find $\alpha_1 = 0, \alpha_2 < 0$ by solving $\mathrm{tr}(J) = 0, \det(J) > 0$. Note that the to bifurcation curves meet at $(\alpha_1, \alpha_2) = (0, 0)$. This becomes clear when we see the diagram containing these bifurcation curves and the Bogdanov-Takens point, as in figure 9. △

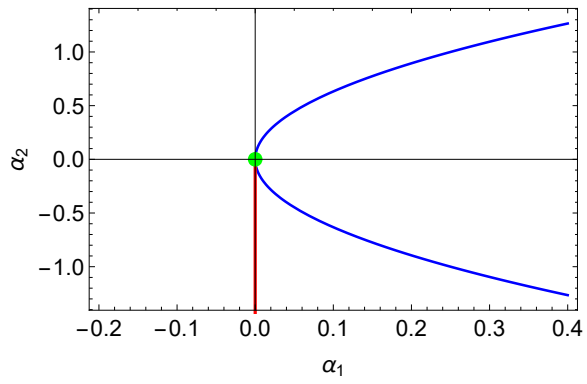

Figure 9: Bifurcation diagram of system (34) in the (α_1, α_2)-plane. The blue curve corresponds to the fold bifurcation, the red curve is of the Hopf bifurcation, and the orange point is the Bogdanov-Takens bifurcation.

Remark. A diagram in the parameter space containing bifurcation curves and points, is often called a bifurcation diagram. Different enclosed regions in this diagram, correspond to different phase portraits (in terms of topological equivalence). ♢

1.2.4 Bifurcations of periodic orbits

So far, we have focused on bifurcations of equilibria. At these bifurcations, the number and/or stability of equilibria changed, leading to topologically nonequivalent systems. However, as we discussed earlier in this section, also for periodic orbits (cycles) there is a notion of stability. By adding parameters, also the number and/or stability of cycles might change under variation of these parameters. In that way one could encounter bifurcations of periodic orbits. We could repeat the whole bifurcation theory for cycles, we will however give one example (for other bifurcations of cycles we refer to [15], we will not need them for the purpose of this project).
We will study the analogy of the fold bifurcation, in the setting of periodic orbits. We are back in the setting with one parameter $\alpha \in \mathbb{R}$, in a dynamical system of the form

$$\dot{x} = f(x, \alpha) \tag{37}$$

and $x \in \mathbb{R}^n$, $f : \mathbb{R}^n \times \mathbb{R} \to \mathbb{R}^n$ a smooth function. We assume the system has a hyperbolic cycle $\mathcal{C}$ for some parameter value α_0. This means that for $x_0 \in \mathcal{C}$, the Poincaré map has multipliers (eigenvalues of Jacobian) $|\mu| \neq 1$. By changing the parameter α, it might happen that one of the multipliers becomes $\mu_1 = 1$. Then the new system will be topologically nonequivalent, leading to a bifurcation.

Definition 1.17. Suppose that at some value of α, one multiplier of the Poincaré map becomes $\mu_1 = 1$. This is called a *cycle fold* bifurcation. △

Remark. The cycle fold bifurcation is also called *limit point of cycles* or *cycle saddle-node* bifurcation. ♢

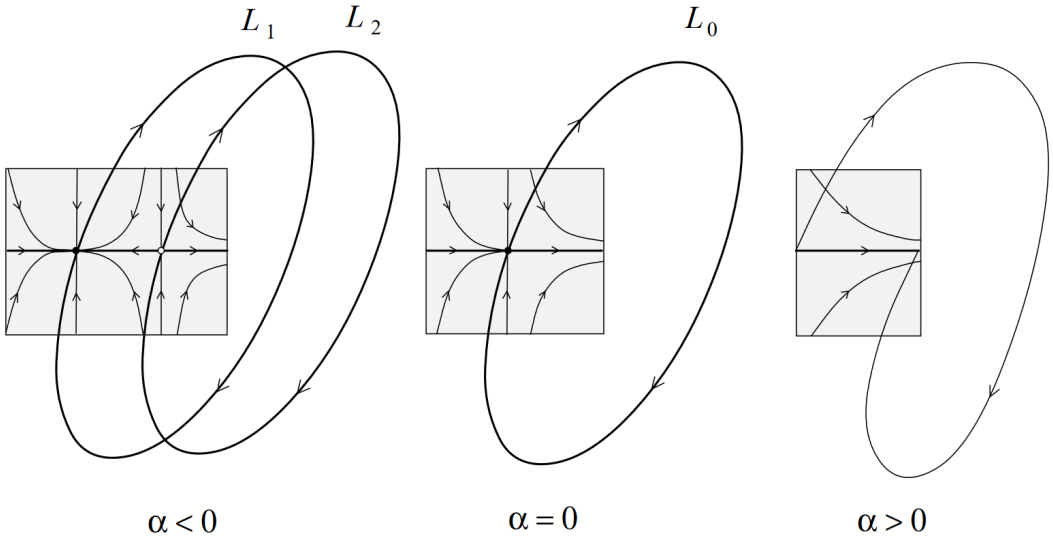

Figure 10: Sketch of a cycle fold bifurcation at $\alpha = 0$. Figure from [15].

In figure 10, a sketch is given of a cycle fold bifurcation. It is analogous to a fold bifurcation of equilibria: two cycles L_1 (stable) and L_2 (unstable) collide at the bifurcation point $\alpha = \alpha_0 = 0$ and disappear. We will not try to find this bifurcation analytically, since it is usually rather hard to find an explicit formula of a Poincaré map of a cycle. There are ways to detect this bifurcation, as also other cycle bifurcations and equilibrium bifurcations, numerically. An example of software to do this with, is MATCONT [16], which will be used later on.
There are also other codim 1 bifurcations of cycles, and bifurcations of higher codimension, as in the case of bifurcations of equilibria. However very interesting, we will not study these types of bifurcations here.

1.3 Tipping points in dynamical systems

1.3.1 Time dependent dynamical systems

So far, we studied dynamical systems defined by autonomous (first order) ODEs. We will now study systems that can depend explicitly on time, which are called nonautonomous systems. This time dependence will be incorporated via the parameter set. In the general setting, we have dynamical systems on $\mathbb{R}^n$,

$$\dot{x} = f(x, \alpha(t)) \tag{38}$$

with the parameters now a smooth function $\alpha : \mathbb{R} \to \mathbb{R}^s$ of t and the function $f : \mathbb{R}^n \times \mathbb{R}^s \to \mathbb{R}^n$ also smooth. The smoothness implies that the eigenvalues not only continuously depend on the parameter value, but now also continuously on time. Phase portraits will now be difficult to draw, since the corresponding vector field changes in time. For every time t, we could draw a vector field (like taking a photograph), but as this field changes over time, it does not actually consists of the orbits (and is therefore not a phase portrait). However, given an initial condition $x_0 \in \mathbb{R}^n$ at time $t = t_0 \in \mathbb{R}$, we can still speak of the corresponding solution $x(t; x_0, t_0)$. It could still be that a solution converges towards an equilibrium. However, because of the time dependence, this equilibrium might change position or stability in time. These changes in equilibria are similar to bifurcations, and can be observed in solutions of the system. These qualitative changes of the solution (in time), are referred to as *tipping points*, which will be discussed in the next paragraph.

1.3.2 Tipping points

In many different research areas, one speaks about tipping points. Also in popular science literature you can come across this terminology. However, not everyone means the same when they are talking about tipping points. In this paragraph, we will give a definition in the mathematical setting as discussed so far. Also in mathematics, you can define different kinds of tipping points [17]. We will focus on tipping points that are *induced* by bifurcations.
We will investigate the possibilities of tipping points in a systems as described in equation

(38). Let $x(t; x_0, t_0)$ denote the solution of the system with initial condition $x(t_0; x_0, t_0) = x_0$, and we assume this solution to be valid on some time-interval $I \subset \mathbb{R}$. We will give conditions for a tipping point to be present in this solution.

Definition 1.18. Suppose there exists $t^* \in I$ such $\alpha^* = \alpha(t^*)$ is a bifurcation point of the autonomous system $\dot{x} = f(x, \alpha^*)$. Then this $t^* \in I$ is called a *tipping point* of the solution $x(t; x_0, t_0)$. △

Example 1.7. Consider the time dependent planar dynamical system

$$\begin{cases} \dot{x} &= (t-2)x \\ \dot{y} &= -y \end{cases} \tag{39}$$

with an equilibrium at the origin and corresponding Jacobian matrix

$$J = \begin{pmatrix} t-2 & 0 \\ 0 & -1 \end{pmatrix} \tag{40}$$

which also depends on time. Defining $\alpha(t) = t - 2$, the first equation can be written as $\dot{x} = \alpha(t)x$. At $t = 2$, we have $\det(J) = 0$ and therefore a fold bifurcation in the corresponding autonomous system given by

$$\begin{cases} \dot{x} = \alpha x \\ \dot{y} = -y \end{cases} \tag{41}$$

and thus $t = 2$ is a tipping point of any solution of (39). For $t < 2$, both eigenvalues are negative implying that the equilibrium is stable. However, the origin becomes unstable for $t > 2$. Since this is a rather simple system, the equations can be solved analytically. When taking as initial condition $t_0 = 0$, $x_0 = 1$, $y_0 = 1$, we find the solution

$$(x(t; 1, 0), y(t; 1, 0)) = \left(e^{-2t+\frac{1}{2}t^2}, e^{-t}\right) \tag{42}$$

which is plotted in figure 11. We indeed see both x and y converging to 0 for $t < 2$, and x diverging for larger t. △

Example 1.8. We consider a time dependent variant of the dynamical system of example 1.4, with parameter function

$$\alpha = \alpha(t) = \tanh\left(\frac{t-10}{10}\right) \tag{43}$$

i.e. we are studying the planar system described by

$$\begin{cases} \dot{x} &= \tanh\left(\frac{t-10}{10}\right) x - y - x(x^2+y^2) \\ \dot{y} &= x + \tanh\left(\frac{t-10}{10}\right) y - y(x^2+y^2) \end{cases} \tag{44}$$

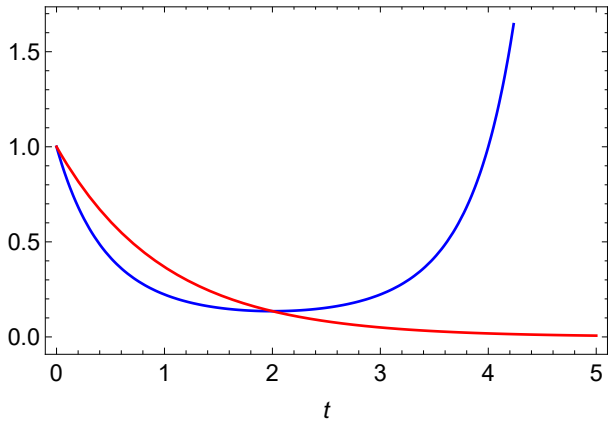

Figure 11: Solution curves of $x(t;1,0)$ (blue) and $y(t;1,0)$ (red) of system (39).

of which the origin is an equilibrium and observe that the Jacobian matrix at the origin is given by

$$J = \begin{pmatrix} \tanh\left(\frac{t-10}{10}\right) & -1 \\ 1 & \tanh\left(\frac{t-10}{10}\right) \end{pmatrix} \tag{45}$$

and recall that the autonomous system undergoes a supercritical Hopf bifurcation at $\alpha = 0$. Now consider a solution of the system, e.g. $(x(t;\frac{1}{2},0), y(t;-\frac{1}{2},0)$ with initial condition $(x_0, y_0) = (\frac{1}{2}, -\frac{1}{2})$. We expect a tipping point at $t = 10$, since that corresponds to $\alpha = \tanh(0) = 0$. For $t < 10$, the origin is stable (since $\alpha < 0$) and for $t > 10$ ($\alpha > 0$) we expect oscillatory behavior (since the autonomous system has a stable cycle). We can indeed see these features in the graphs of x and y in figure 12. △

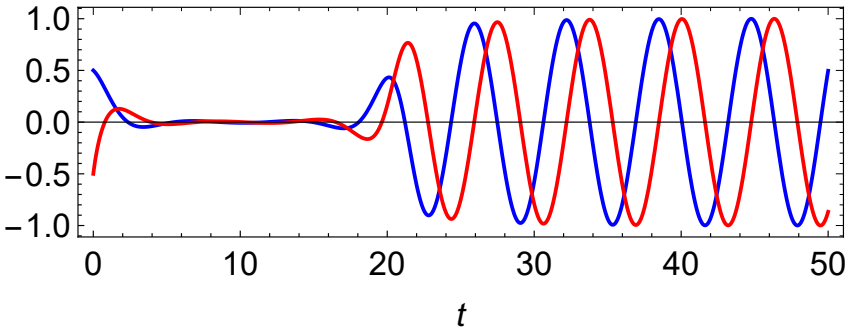

Figure 12: Solution curves of $x(t;\frac{1}{2},0)$ (blue) and $y(t;-\frac{1}{2},0)$ (red) of system (44).

Remark. Whether we see the (bifurcation induced) tipping point in the solution of the system, depends on the way the parameter(s) depend on time. The 'speed' in which the parameters change is important, and also the presence of noise can have influence. ♢

2 MPT in the Saltzman-Maasch model

In this chapter, we will investigate a conceptual climate model of the last few million years. The model was proposed by Saltzman and Maasch in 1991 [1] and is one of a series of conceptual models of these researchers. This particular ODE model is a slightly modified version of the model they had proposed a year earlier [18]. The dynamical system is a simple set of three differential equations, describing changes in the global ice mass (I), atmospheric CO_2 concentration (μ) and (a measure of) the deep ocean circulation (θ). The precise description of the system is given by

$$\begin{cases} \dot{I} &= \alpha_1 - c\alpha_2\mu - \alpha_3 I - k_\theta\alpha_2\theta - k_R\alpha_2 F_I \\ \dot{\mu} &= \beta_1 - (\beta_2 - \beta_3\mu + \beta_4\mu^2)\mu - \beta_5\theta + F_\mu \\ \dot{\theta} &= \gamma_1 - \gamma_2 I - \gamma_3\theta \end{cases} \tag{46}$$

where $\{\alpha_i, \beta_j, \gamma_k\}_{i,j,k=1,2,\ldots}$ is the set of parameters, which link the state variables I, μ and θ to each other. $F_I = F_I(t)$ and $F_\mu = F_\mu(t)$ are functions that describe the (time dependent) forcing. The constants c, k_θ and k_R are determined from equilibrium climate model simulations that relate the temperature (via the parameter α_2) to atmospheric CO_2 concentration, deep ocean temperature and incoming solar radiation.
Our goal is to find tipping points that affect the solutions of the model in such a way that we can simulate MPT behavior. The results of the first chapter come in handy, but in order to use them we first have to make sure the system is in the setting of dynamical systems. We will derive a non-dimensional autonomous version of the model. Then we study a 2D simplification of this model, and of the non-dimensional 3D model. This is in both cases done with a bifurcation analysis. When we know the bifurcation structure, we can find tipping points by letting one or more parameters be time dependent and we can simulate the MPT in such a model. Lastly, we will use the knowledge of the non-dimensional model to simulate the MPT in the full Saltzman-Maasch model.

2.1 Derivation of the non-dimensional model

We will decompose the state variables as

$$\begin{pmatrix} I \\ \mu \\ \theta \end{pmatrix} = \begin{pmatrix} I_0 \\ \mu_0 \\ \theta_0 \end{pmatrix} + \begin{pmatrix} I' \\ \mu' \\ \theta' \end{pmatrix} \tag{47}$$

where (I_0, μ_0, θ_0) is the background climate (long term tectonic equilibrium) and we refer to (I', μ', θ') as the deviation to the this background state. Furthermore, we also write $F_I = \bar{F}_I + F_I'$ and we assume $F_\mu = 0$, i.e. we only consider forcing in the equation for I. For the background state we now know that

$$\begin{cases} 0 = & \alpha_1 - c\alpha_2\mu_0 - \alpha_3 I_0 - k_\theta\alpha_2\theta_0 - k_R\alpha_2\bar{F}_I \\ 0 = & \beta_1 - (\beta_2 - \beta_3\mu_0 + \beta_4\mu_0^2)\mu_0 - \beta_5\theta_0 \\ 0 = & \gamma_1 - \gamma_2 I_0 - \gamma_3\theta_0 \end{cases} \tag{48}$$

We can also plug (47) into the original system (46) to get

$$\begin{cases} \dot{I}' &= \alpha_1 - c\alpha_2(\mu_0 + \mu') - \alpha_3(I_0 + I') - k_\theta\alpha_2(\theta_0 + \theta') - k_R\alpha_2(\bar{F}_I(t) + F'(t)) \\ \dot{\mu}' &= \beta_1 - (\beta_2 - \beta_3(\mu_0 + \mu') + \beta_4(\mu_0 + \mu')^2)(\mu_0 + \mu') - \beta_5(\theta_0 + \theta') \\ \dot{\theta}' &= \gamma_1 - \gamma_2(I_0 + I') - \gamma_3(\theta_0 + \theta') \end{cases} \tag{49}$$

and using (48) we can reduce this to

$$\begin{cases} \dot{I}' &= -c\alpha_2\mu' - \alpha_3 I' - k_\theta\alpha_2\theta' - k_R\alpha_2 F'(t) \\ \dot{\mu}' &= b_1\mu' - b_2\mu'^2 - \beta_4\mu'^3 - \beta_5\theta' \\ \dot{\theta}' &= -\gamma_2 I' - \gamma_3\theta' \end{cases} \tag{50}$$

where we introduced the new parameters

$$b_1 = -\beta_2 + 2\beta_3\mu_0 - 3\beta_4\mu_0^2, \qquad b_2 = -\beta_3 + 3\beta_4\mu_0 \tag{51}$$

to simplify the equations. Note that these new parameters depend only on previous parameters of the μ-equation and on μ_0, which can be thought of as a reference value for the CO_2 concentration. Now we non-dimensionalise the equations by the mappings

$$\begin{cases} t &\mapsto \lambda_0 t^* \\ I' &\mapsto \lambda_1 X \\ \mu' &\mapsto \lambda_2 Y \\ \theta' &\mapsto \lambda_3 Z \end{cases} \tag{52}$$

where the different scales are given by

$$\lambda_0 = \frac{1}{c\alpha_2}, \qquad \lambda_1 = \frac{c\alpha_2}{\sqrt{\alpha_3\beta_4}}, \qquad \lambda_2 = \sqrt{\frac{\alpha_3}{\beta_4}}, \qquad \lambda_3 = \frac{c\alpha_2\gamma_2}{\gamma_3\sqrt{\alpha_3\beta_4}}. \tag{53}$$

The obtained dimensionless dynamical system is then

$$\begin{cases} \dot{X} &= -X - Y - vZ - uF_I'(t^*) \\ \dot{Y} &= -pZ + rY - sY^2 - Y^3 \\ \dot{Z} &= -q(X + Z) \end{cases} \tag{54}$$

where the dot now represents the derivative with respect to the new time t^*, which we will call t again from now on. The parameters $p, q, r, s, u, v \in \mathbb{R}$ depend on the previous set $\{\alpha_i, \beta_j, \gamma_k\}_{i,j,k=1,2,\ldots}$ of (dimensional) parameters. The parameter space is six-dimensional, which we will first reduce even further when investigating a simplified version of the model. For a bifurcation analysis, we will look at the autonomous system, i.e. ignoring the forcing term $F_I'(t)$ (or equivalently, setting $u = 0$). The analysis of the simplified 2D model helps to understand the dynamics of the system, with the most important parameters. This can help understand the dynamics of the 3D model (with 6 parameters).

2.2 Analysis of the simplified 2D model

For the simplest case that we will consider, we set, apart from $u = 0$, also $s = v = 0$ and let $q \to \infty$. The last condition implies $Z = -X$, i.e. the model reduces to a planar dynamical system. In physical terms, we assume that on longer time scales, ice volume and deep ocean temperature are in anti-phase. The dynamical system is then described by

$$\begin{cases} \dot{X} &= -X - Y \\ \dot{Y} &= pX + rY - Y^3 \end{cases} \tag{55}$$

which now only consists of two parameters. Note that there is $\mathbb{Z}_2$ symmetry in the system (for $(X, Y) \mapsto (-X, -Y)$). The equilibria of this system are located at $\{(0,0), (\sqrt{r-p}, -\sqrt{r-p}), (-\sqrt{r-p}, \sqrt{r-p})\}$. Note that the nontrivial equilibria only exist for $r > p$. This already suggests that a bifurcation takes place at $p = r$. For further investigation of this (and other bifurcations), consider the Jacobian matrix J at the origin, given by

$$J(0,0) = \begin{pmatrix} -1 & -1 \\ p & r \end{pmatrix} \tag{56}$$

Recall that this equilibrium has a fold bifurcation when $\det J(0,0) = 0$, which is indeed at $p = r$. Furthermore, $\mathrm{tr} J(0,0) = 0$ when $r = 1$. The eigenvalues $\lambda_{1,2}$ of this Jacobian matrix are given by

$$\lambda_{1,2} = \frac{r-1}{2} \pm \frac{1}{2}\sqrt{(r-1)^2 - 4(p-r)} \tag{57}$$

and we see that a Hopf bifurcation happens at $r = 1$, for $p > r$. The Hopf bifurcation is supercritical. For $p < r$, we also have $\lambda_1 + \lambda_2 = 0$, but the eigenvalues are real instead of imaginary. This is called a neutral saddle. A special point in parameter space is in this case $p = r = 1$, where both eigenvalues equal zero. This corresponds to a Bogdanov-Takens bifurcation.

To find bifurcations of the nontrivial equilibria, we look at the Jacobian matrix evaluated at those points,

$$J(\pm\sqrt{r-p}, \mp\sqrt{r-p}) = \begin{pmatrix} -1 & -1 \\ p & 3p - 2r \end{pmatrix} \tag{58}$$

which has eigenvalues

$$\lambda_{1,2} = \frac{3p - 2r - 1}{2} \pm \frac{1}{2}\sqrt{(3p - 2r - 1)^2 - 8(r-p)} \tag{59}$$

and we see that a Hopf bifurcation occurs when $3p - 2r - 1 = 0$, or equivalently, $r = \frac{3p-1}{2}$. The bifurcation is subcritical. This is a curve in the (p, r)-plane, and together with the

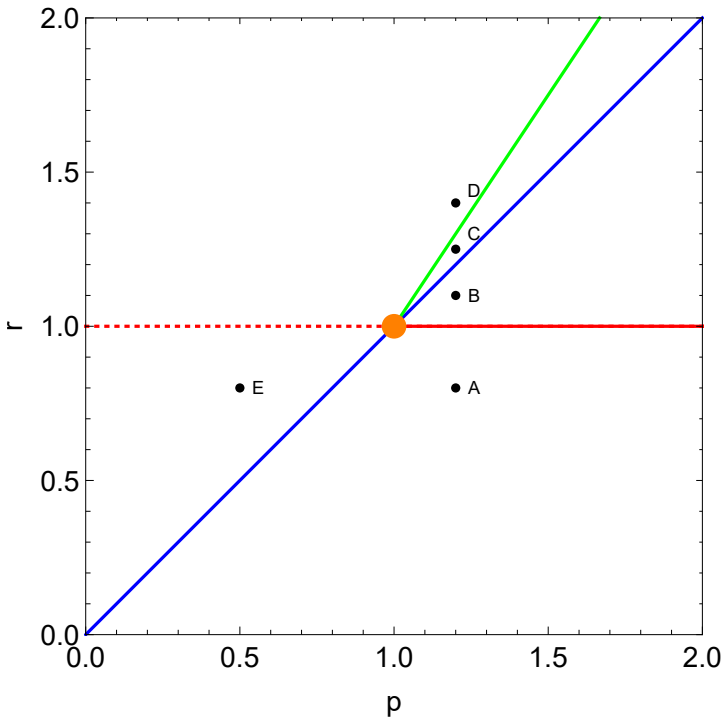

Figure 13: Bifurcation diagram of (55) in the (p, r)-plane. Blue line: fold bifurcation, red solid line: Hopf bifurcation of $(0, 0)$, red dotted line: neutral saddle, orange point: Bogdanov-Takes bifurcation, green line: Hopf bifurcation of nontrivial equilibria.

bifurcations we found for the trivial equilibrium, they form a bifurcation diagram. This diagram is plotted in figure 13.

Using the `pplane9` software in Matlab, we can visualize the phase portraits for different points in the parameter space. The points for which this is done, are the black dots in figure 13, labeled A through E. For $p = 1.2$, the phase portraits (i.e. of points A-D) are shown in figure 14. The phase portrait at point E is shown in figure 15. Although this is a different point in parameter space, from 13 one would expect a similar phase portrait as at point D, since the points are not separated by any bifurcation curves. This is indeed the case.

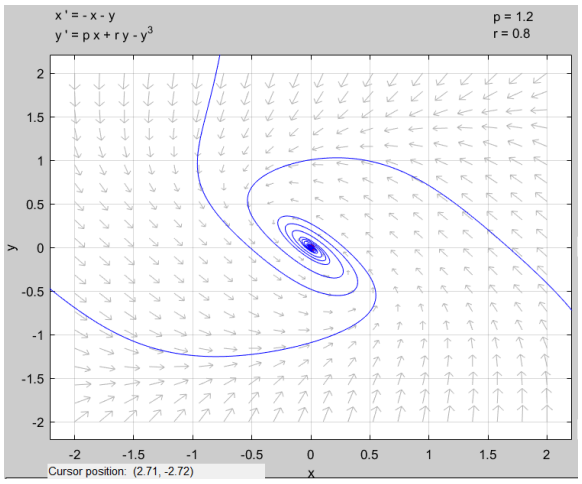

(a) Phase portrait for $(p, r) = (1.2, 0.8)$. The origin is stable.

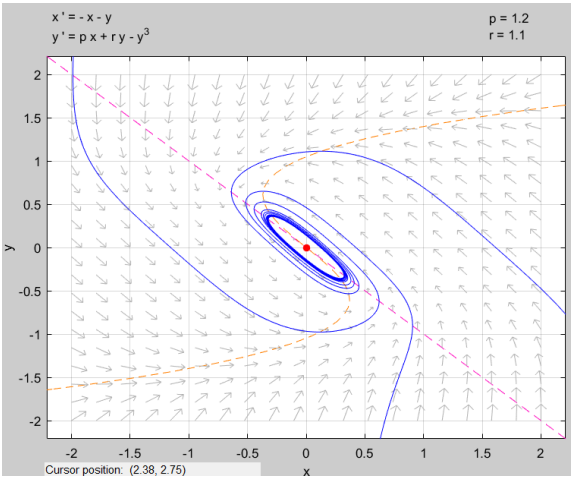

(b) Phase portrait for $(p, r) = (1.2, 1.1)$. The origin is unstable, and a limit cycle has emerged (due to Hopf bifurcation).

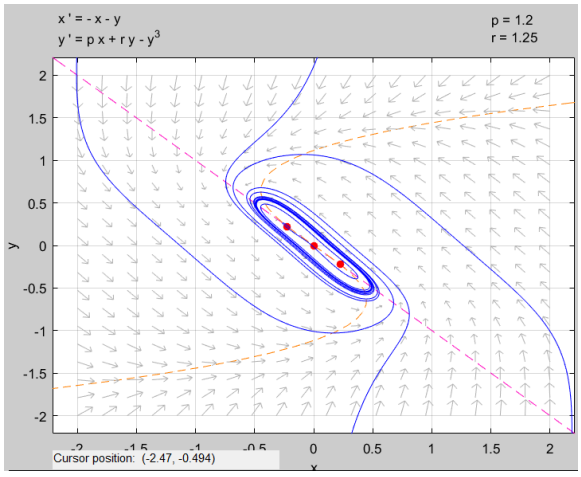

(c) Phase portrait for $(p, r) = (1.2, 1.25)$. The nontrivial equilibria have appeared and are unstable, the origin is a saddle. The limit cycle encloses all equilibria.

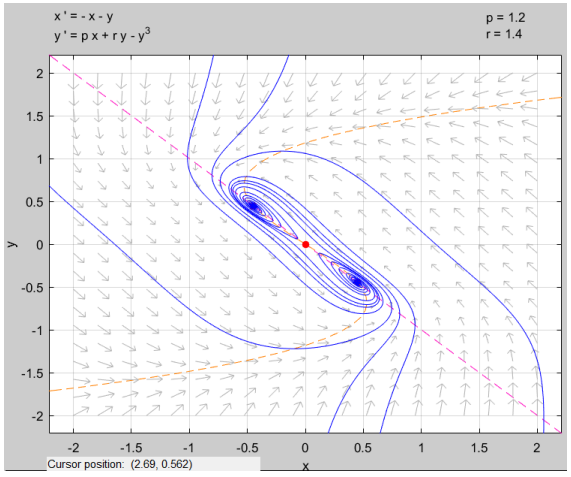

(d) Phase portrait for $(p, r) = (1.2, 1.4)$. The limit cycle has disappeared (due to subcritical Hopf bifurcation), the nontrivial equilibria are stable and the origin is a saddle.

Figure 14: Different phase portraits for varying values of r (and fixed $p = 1.2$).

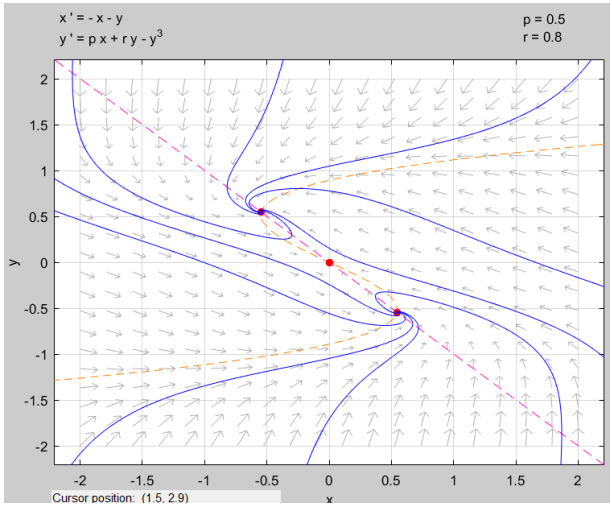

Figure 15: Phase portrait for $(p, r) = (0.5, 0.8)$. Stable nontrivial equilbria, the origin is a saddle. This is topologically equivalent to figure 14(d).

Now let $v > 0$ be nonzero (and it is by definition positive). The system in equation (55) then becomes

$$\begin{cases} \dot{X} &= (v-1)X - Y \\ \dot{Y} &= pX + rY - Y^3 \end{cases} \tag{60}$$

which is still symmetric. The equilibria are now located at

$$\left\{(0,0), \left(\sqrt{\frac{p+r(v-1)}{(v-1)^3}}, \sqrt{r+\frac{p}{v-1}}\right), \left(-\sqrt{\frac{p+r(v-1)}{(v-1)^3}}, -\sqrt{r+\frac{p}{v-1}}\right)\right\} \tag{61}$$

and the Jacobian at the origin is given by

$$J(0,0) = \begin{pmatrix} v-1 & -1 \\ p & r \end{pmatrix} \tag{62}$$

With a similar analysis we find for example the fold bifurcation ($\det J(0,0) = 0$) when $r(v-1)+p = 0$, which defines a curve in the three dimensional (p, r, v) parameter space. Looking at the eigenvalues, given by

$$\lambda_{1,2} = \frac{v-1+r}{2} \pm \frac{1}{2}\sqrt{(v-1+r)^2 - 4(p+r(v-1))} \tag{63}$$

we again find a Hopf bifurcation, now when $v-1+r = 0$ and $p+r(1-v)$, i.e. if $r = 1-v$ and $p > (v-1)^2$. Qualitatively, the bifurcation diagram in the (p, r)-plane remains the same as in figure 13, only the position of the codim 2 Bogdanov-Takens bifurcation point now depends on v. Following [1], we can fix $v = \frac{1}{5}$. The fold bifurcation curve in the (p, r)-plane is then at $p = \frac{4}{5}r$, and the Hopf curve at $r = \frac{4}{5}$, for $p > \frac{16}{25}$. The point $(\frac{16}{25}, \frac{4}{5})$

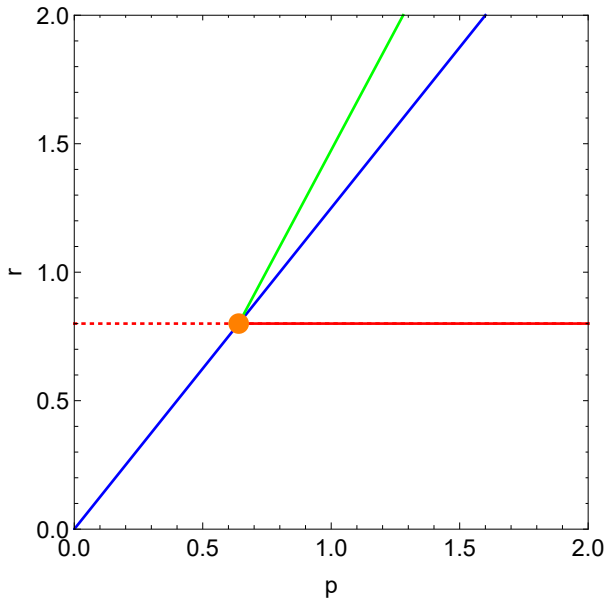

Figure 16: Bifurcation diagram of (60) in the (p, r)-plane, for $v = \frac{1}{5}$. Blue line: fold bifurcation, red solid line: Hopf bifurcation of $(0, 0)$, red dotted line: neutral saddle, orange point: Bogdanov-Takens bifurcation, green line: Hopf bifurcation of nontrivial equilibria.

is now the new position of the codim 2 Bogdanov-Takens bifurcation point. The new bifurcation diagram is plotted in figure 16.
We indeed see that the bifurcation diagram is qualitatively the same as before. The Bogdanov-Takens point is the so-called 'organizing center' in the bifurcation diagram. As soon as you know the position of this point, the codim 1 curves emerge from this and you can deduce the dynamics of the system.

2.3 Analysis of the 3D model

In the 2D model, we have seen that the parameters of the Y equation (in that case p and r) already determine a lot of the dynamics (and bifurcations) of the system. In this paragraph, we return to the 3D non-dimensional autonomous dynamical system as described in equation (54). The equilibria can be found analytically: except for $(\bar{X}_0, \bar{Y}_0, \bar{Z}_0) = (0, 0, 0)$ there are two more, given by

$$(\bar{X}_1, \bar{Y}_1, \bar{Z}_1) = \left(-\frac{s}{2(v-1)} - \frac{Q}{2(v-1)^{3/2}}, -\frac{s}{2} - \frac{Q}{2\sqrt{v-1}}, \frac{s}{2(v-1)} + \frac{Q}{2(v-1)^{3/2}} \right) \quad (64)$$

and

$$(\bar{X}_2, \bar{Y}_2, \bar{Z}_2) = \left(-\frac{s}{2(v-1)} + \frac{Q}{2(v-1)^{3/2}}, -\frac{s}{2} + \frac{Q}{2\sqrt{v-1}}, \frac{s}{2(v-1)} - \frac{Q}{2(v-1)^{3/2}} \right). \quad (65)$$

In these equations we used Q as an abbreviation of $Q = \sqrt{4p + (4r + s^2)(v - 1)}$. We will analyze the system, in particular the bifurcations of these equilibria, by varying two parameters (and letting the others fixed). As in the 2D system, we will focus on the Y equation. We will investigate bifurcations when varying (r, s) and for (p, r).

We start by doing a numerical bifurcation analysis, with three fixed parameters: $p = 1, q = 2.5, v = 0.2$. For the analysis we then have two 'active' parameters, r and s (i.e. these are allowed to vary). Using the bifurcation software `MATCONT` for Matlab, we can make a bifurcation diagram in the (r, s)-plane, for $(r, s) \in [0, 3] \times [0, 3]$. The result is shown in figure 17.

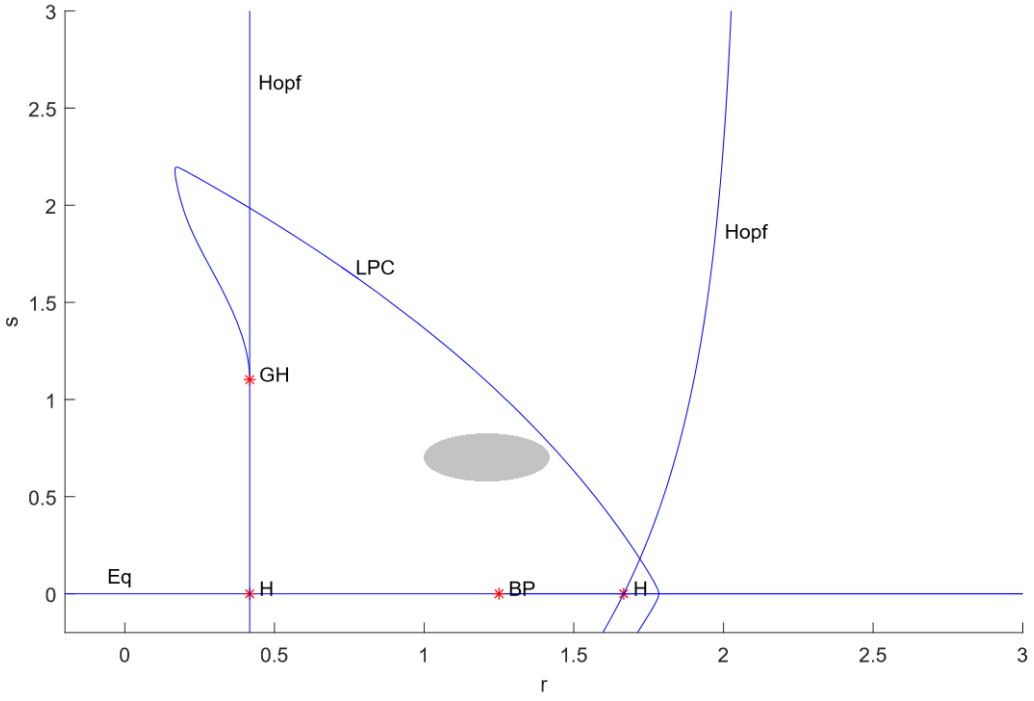

Figure 17: Bifurcation diagram in the (r, s)-plane. The left Hopf curve is of the origin, the right one is of the nontrivial equilibria. In the grey area, solutions have a period of ≈ 100 kyr.

At four different positions in the (r, s)-plane, a phase portrait is constructed. The results are shown in figure 18. We see that in some regions a limit cycle is present, and also its stability can change. This is all due to the Hopf bifurcation. The LPC curve is the fold (or limit point) bifurcation of the limit cycle.

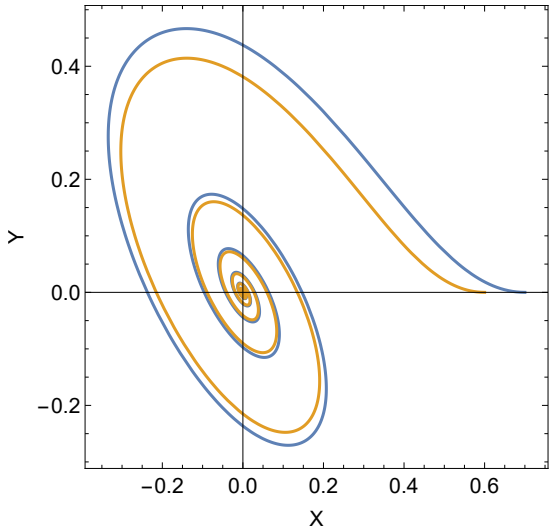

(a) Phase portrait for $(r, s) = (0.2, 0.0)$. The origin is stable.

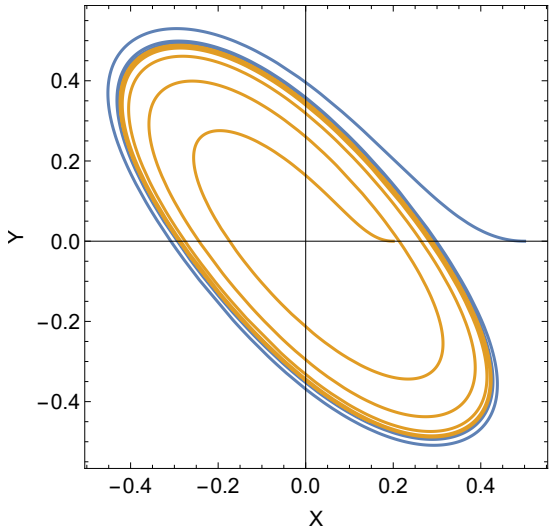

(b) Phase portrait for $(r, s) = (0.6, 0.0)$. The origin is unstable, and a stable limit cycle has emerged (due to Hopf bifurcation).

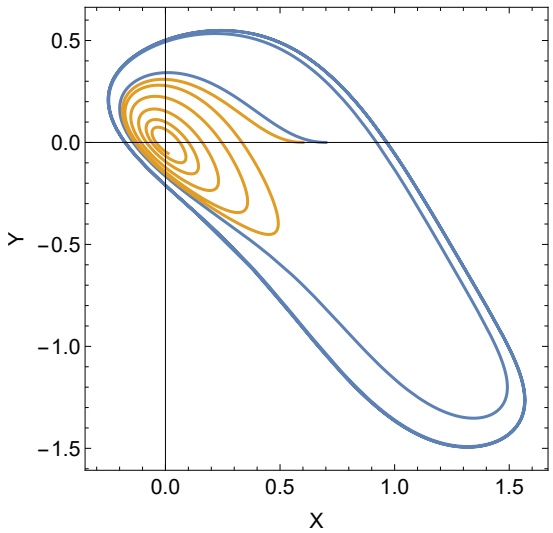

(c) Phase portrait for $(r, s) = (0.3, 1.8)$. The non-trivial equilibria have appeared and are unstable, the origin is stable. Note that not all orbits converge to the limit cycle.

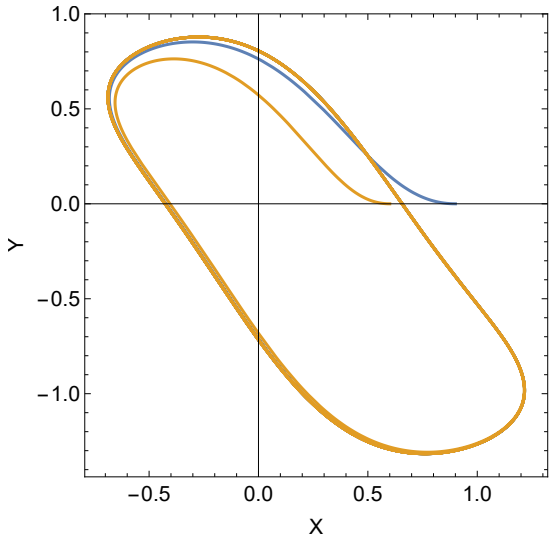

(d) Phase portrait for $(r, s) = (1.3, 0.6)$. Again a stable limit cycle. The period is approximately 100 kyr.

Figure 18: Different phase portraits for varying values of r and s. The different colors indicate a different initial condition. Note that all phase portraits are drawn in the (X, Y)-plane, i.e. the Z-coordinate is neglected.

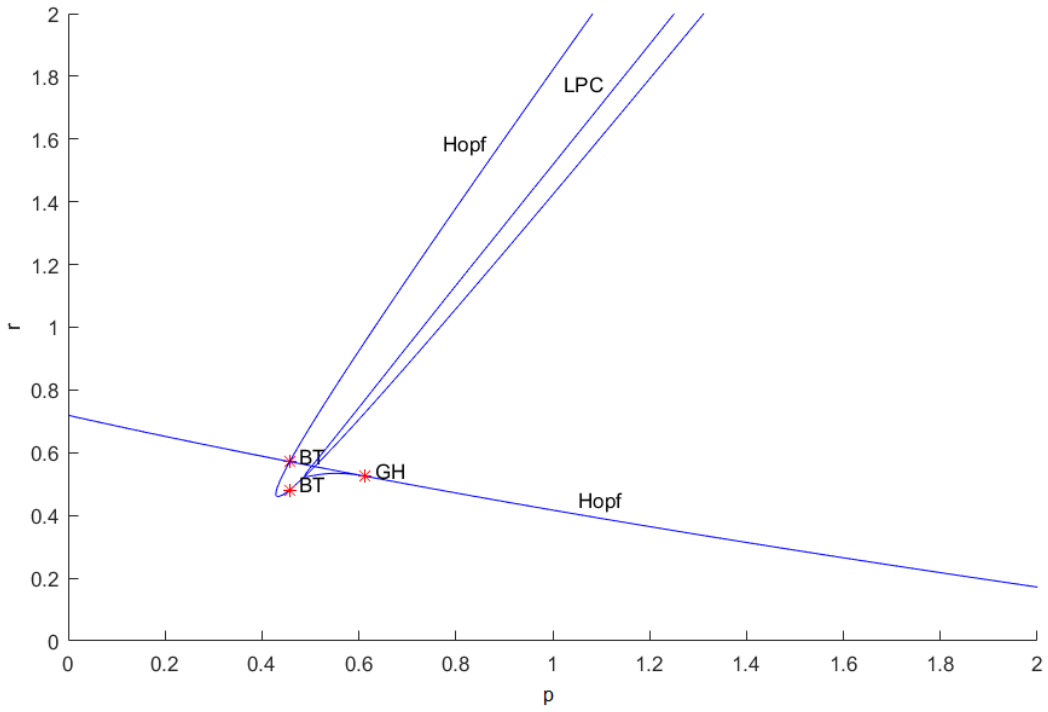

Figure 19: Bifurcation diagram in the (p, r)-plane. The lower Hopf curve is of the origin, the other is of the nontrivial equilibria. In the grey area, solutions have a period of ≈ 100 kyr.

Secondly, we did a similar analysis for varying (p, r). A bifurcation diagram is plotted in the (p, r)-plane (for fixed $s = 0.6$), see figure 19. Although the bifurcation diagram is more complex than in the 2D case (we also have a larger parameter space), we again find the two Hopf curves (trivial and nontrivial), which can lead to the emergence of a limit cycle. We can get from a stable origin state to a limit cycle state, by increasing r. This is the same in both the 2D as the full 3D case. As long as we stay away from the codim 2 bifurcations (BT: Bogdanov Takes, GH: Generalized Hopf/Bautin), we can try to simulate the emergence of an internal oscillation. This is done later on in this chapter.

2.4 Analysis of the full model

We can do a similar bifurcation analysis for the full (i.e. dimensional) Saltzman-Maasch model, as described in equation (46). Note that the parameter space is much larger, but if we only allow one or two parameters to change, we can make a bifurcation diagram. In order to do this, we again have to make the system autonomous. Therefore we set $F_I = F_\mu = 0$. In the non-dimensional models (both 2D and 3D) we have seen that changing one or two parameters in the CO_2 equation are sufficient to encounter Hopf (and other) bifurcations. So we will keep this in mind for the analysis of the full model. For convenience, we will neglect all the units. To start, we take constants $c = 0.004$ and

$k_\theta = 0.04444444$, and set the parameters to

$$\begin{cases} (\alpha_1, \alpha_2, \alpha_3) & = (16.673915, 9.52381, 0.1) \\ (\beta_1, \beta_2, \beta_3, \beta_4, \beta_5) & = (513.4577, 6.25868, 0.02639456, 0.00003628118, 5.833333) \\ (\gamma_1, \gamma_2, \gamma_3) & = (1.85125, 0.01125, 0.25) \end{cases} \tag{66}$$

which is similar to what is done in [19].

We can find one equilibrium numerically, at

$$(I, \mu, \theta) = (35.4722, 281.746, 5.80875) \tag{67}$$

and we will investigate the bifurcations of this equilibrium. This is again done numerically, using the MATCONT software.

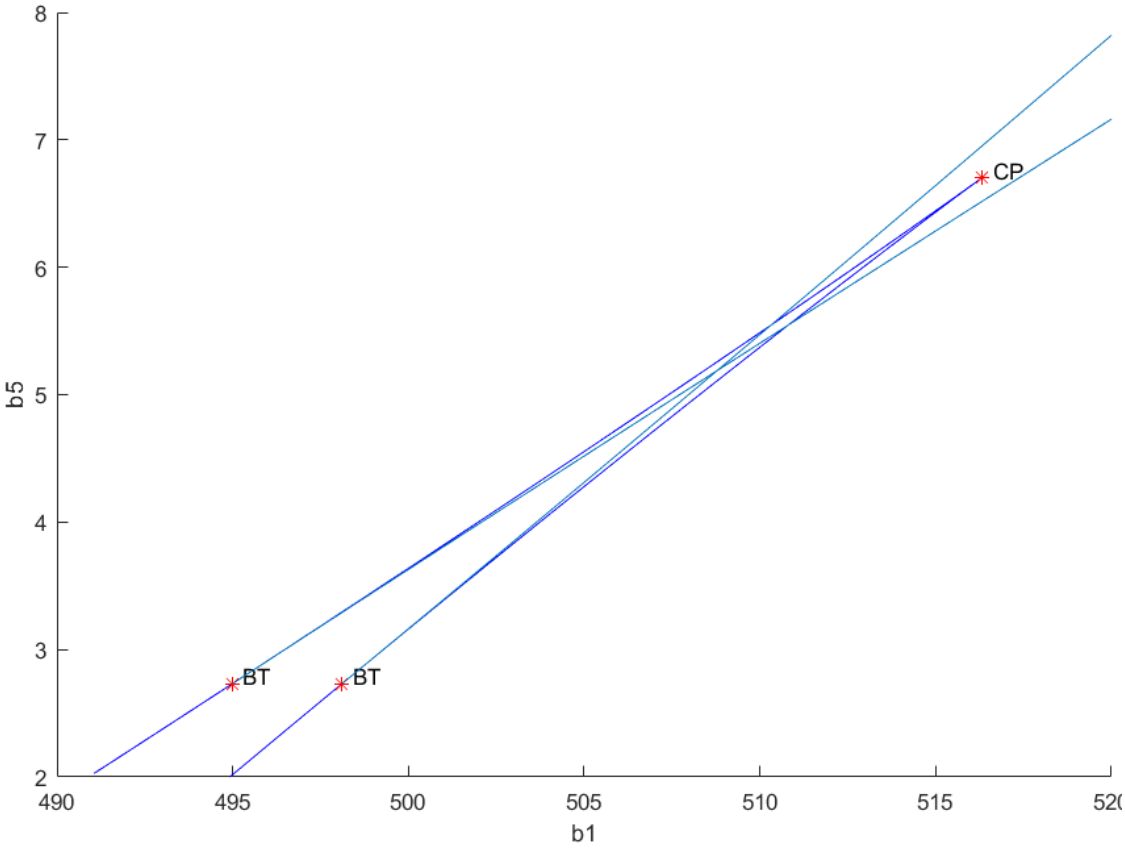

Figure 20: Bifurcation diagram in the (β_1, β_5)-plane. Dark curves are fold bifurcations, light curves are Hopf. BT and CP are codim 2 Bogdanov-Takens and Cusp bifurcations.

We allow two parameters to change, β_1 and β_5. These are the ones that are somehow related to p and r in the non-dimensional models. When we change these parameters, we find both fold and Hopf bifurcations of the equilibrium. The software can continue the bifurcation curves, giving a bifurcation diagram as shown in figure 20. Zooming in closer to the values as given above, gives the diagram as in figure 21. The position of the point where we started, as in equation (66), is to the right of the four curves.

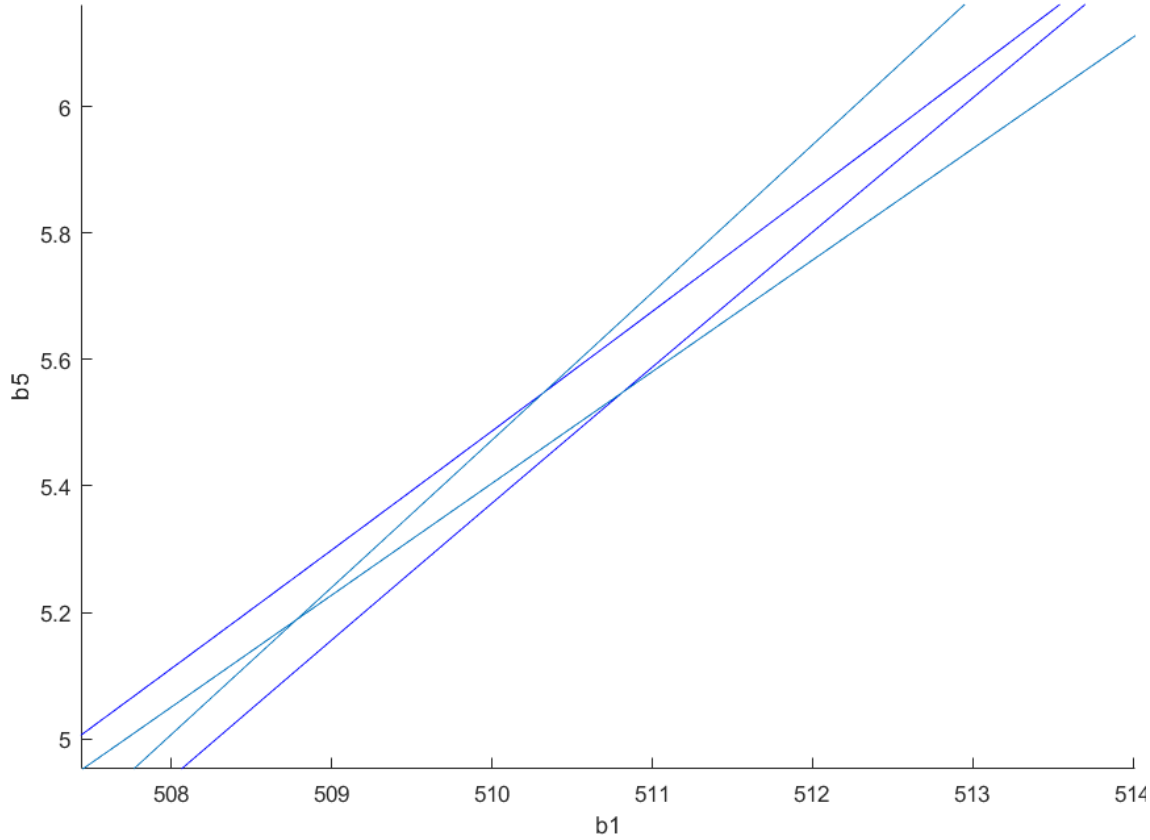

Figure 21: Bifurcation diagram (zoomed in) in the (β_1, β_5)-plane. Dark curves are fold bifurcations, light curves are Hopf.

2.5 Simulation of MPT

In this paragraph, we will use our knowledge of the bifurcation structure of the Saltzman-Maasch model (both non-dimensional and the full model) to simulate MPT behaviour. This is done first for the 3D non-dimensional model.
Looking at the bifurcation diagram in figure 17, we expect that left of the first Hopf curve, there is no internal oscillation, since orbits converge to the origin. When adding a forcing

term (recall that this is the function $F_I'(t)$ in the first differential equation), we can expect a linear response (or close to linear) to the forcing. When crossing the Hopf curve, i.e. when r increases, the system has got a limit cycle and we expect to see that back in the solution. Many different paths through parameter space are possible to achieve MPT-like behaviour, we will show one of them.
We fix $(p, s, q, u, v) = (1.0, 0.6, 2.5, 0.0, 0.2)$. Note that this implies that there is still no forcing present. We let r vary in time, corresponding to

$$r(t) = 0.75 + 0.5 \tanh\left(\frac{t - 1000}{400}\right) \tag{68}$$

of which a graph is shown in figure 22. Note that by defining this function for r, we indeed cross the Hopf bifurcation.

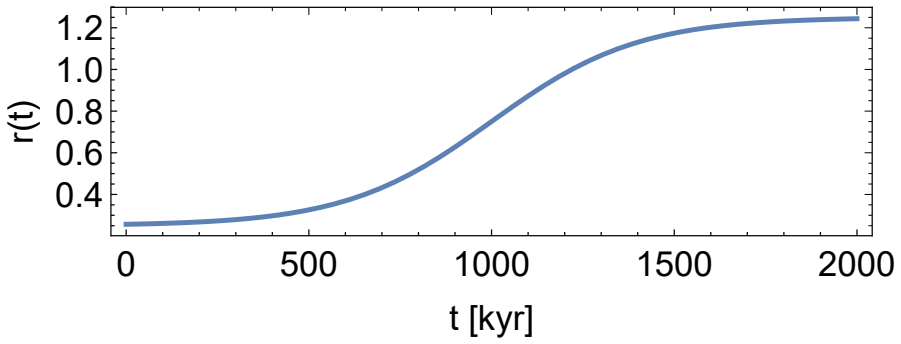

Figure 22: Plot of $r(t)$ as in equation (68).

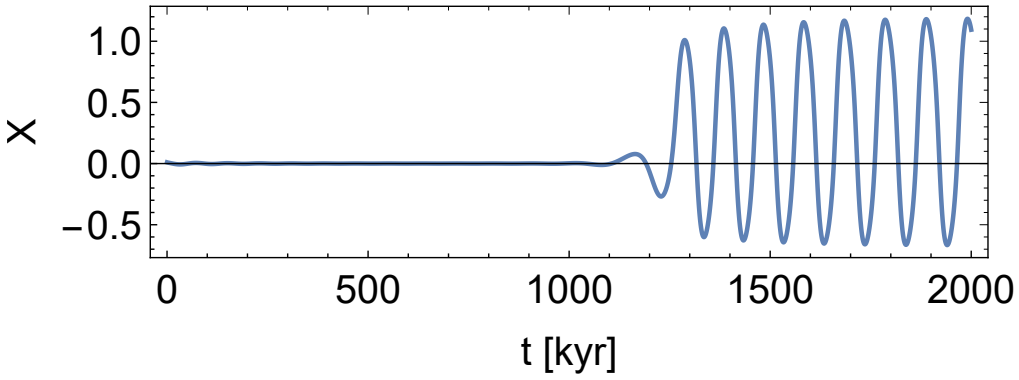

Figure 23: Plot of $X(t)$ for $(p, s, q, u, v) = (1.0, 0.6, 2.5, 0.0, 0.2)$ with $r(t)$ as in equation (68).

With these settings, we simulate the system as in equation (54), starting from $(X(0), Y(0), Z(0)) = (0.1, 0.0, 0.0)$. This yields a graph of $X(t)$ as shown in figure 23. We see that prior to crossing the Hopf curve, no oscillation is present (since the origin is a stable node). After

crossing the bifurcation curve, a limit cycle emerges, which in this case has a period of approximately 100 kyr. Also the other variables go from a stable state to an oscillatory state in a similar way, as can be seen in figure 24.

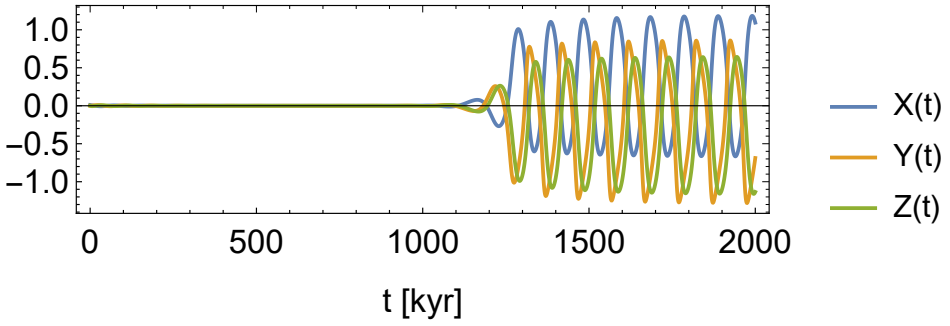

Figure 24: Plot of $X(t)$, $Y(t)$ and $Z(t)$ for $(p, s, q, u, v) = (1.0, 0.6, 2.5, 0.0, 0.2)$ with $r(t)$ as in equation (68).

When we add forcing, we expect that the forcing period will be present prior to the bifurcation (as the autonomous system converges to zero). However, after the bifurcation, we expect a combination of the forcing and the internal oscillation. Therefore we define a purely sinusoidal forcing function,

$$F_I'(t) = \sin\left(\frac{2\pi t}{41}\right) \tag{69}$$

where t is again in kyr. The period of 41 kyr corresponds to the dominant Milankovitch forcing (obliquity). We set $u = 0.6$ and the simulation of $X(t)$ is plotted in figure 25.

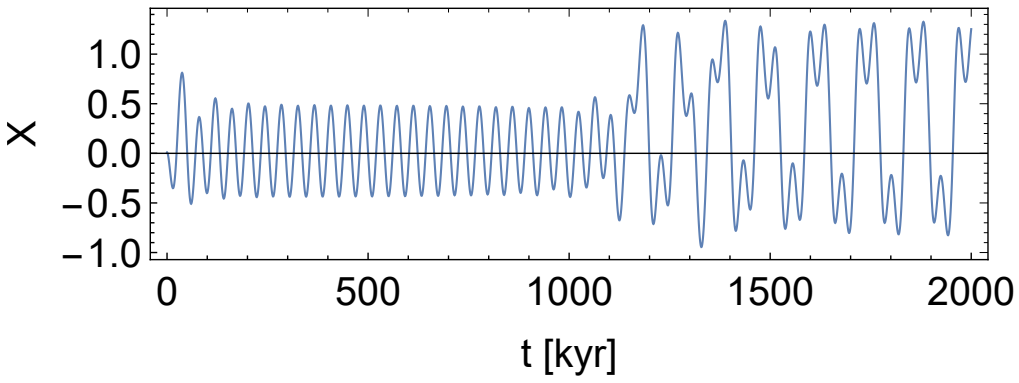

Figure 25: Plot of $X(t)$ for $(p, s, q, u, v) = (1.0, 0.6, 2.5, 0.6, 0.2)$ with $r(t)$ as in equation (68) and $F_I'(t)$ as in equation (69).

To make it more realistic, we also add a second Milankovitch period, namely of 23 kyr.

The forcing function becomes

$$F_I'(t) = \frac{1}{2}\left(\sin\left(\frac{2\pi t}{41}\right) + \sin\left(\frac{2\pi t}{23}\right)\right) \tag{70}$$

and we simulate the system, for $u = 0.7$. The result is shown in figure 26.

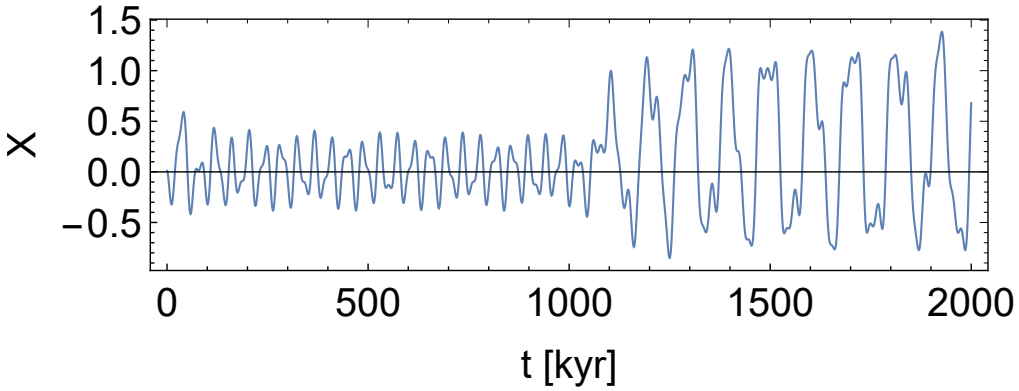

Figure 26: Plot of $X(t)$ for $(p, s, q, u, v) = (1.0, 0.6, 2.5, 0.7, 0.2)$ with $r(t)$ as in equation (68) and $F_I'(t)$ as in equation (70).

We will now simulate the MPT in the full Saltzman-Maasch model. Using the parameters as given in (66), we have found a stable equilibrium (see previous paragraph). Looking at the (close-up) bifurcation diagram in 21, we see that we can cross the Hopf bifurcation curve by decreasing the parameter β_1. By doing this, we can again expect oscillatory behavior in the solutions. We take $\beta_1 = 513.4577$ as starting point, as in equation (66), and let it decrease according to

$$\beta_1 = \beta_1(t) = 513.4577 - \tanh\left(\frac{t}{1000}\right) \tag{71}$$

with t measured in kyr. A graph of this function is plotted in figure 27.

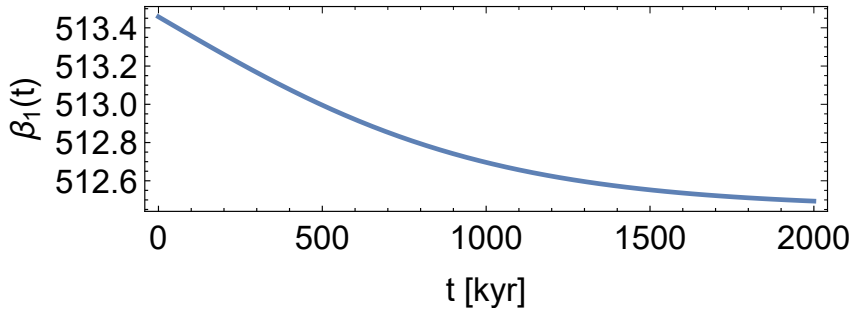

Figure 27: Plot of $\beta_1(t)$ as in equation (71).

The rest of the parameters is held constant. We add a forcing term F_I, given by

$$F_I(t) = \sin\left(\frac{2\pi t}{41}\right) + \sin\left(\frac{2\pi t}{23}\right) \tag{72}$$

with t in kyr (and constant $k_R = 0.1$), i.e. the two dominant Milankovitch cycles. We take $(I, \mu, \theta) = (45, 280, 5.5)$ as initial condition and get a solution for $(I(t), \mu(t), \theta(t))$ as in figure 28.

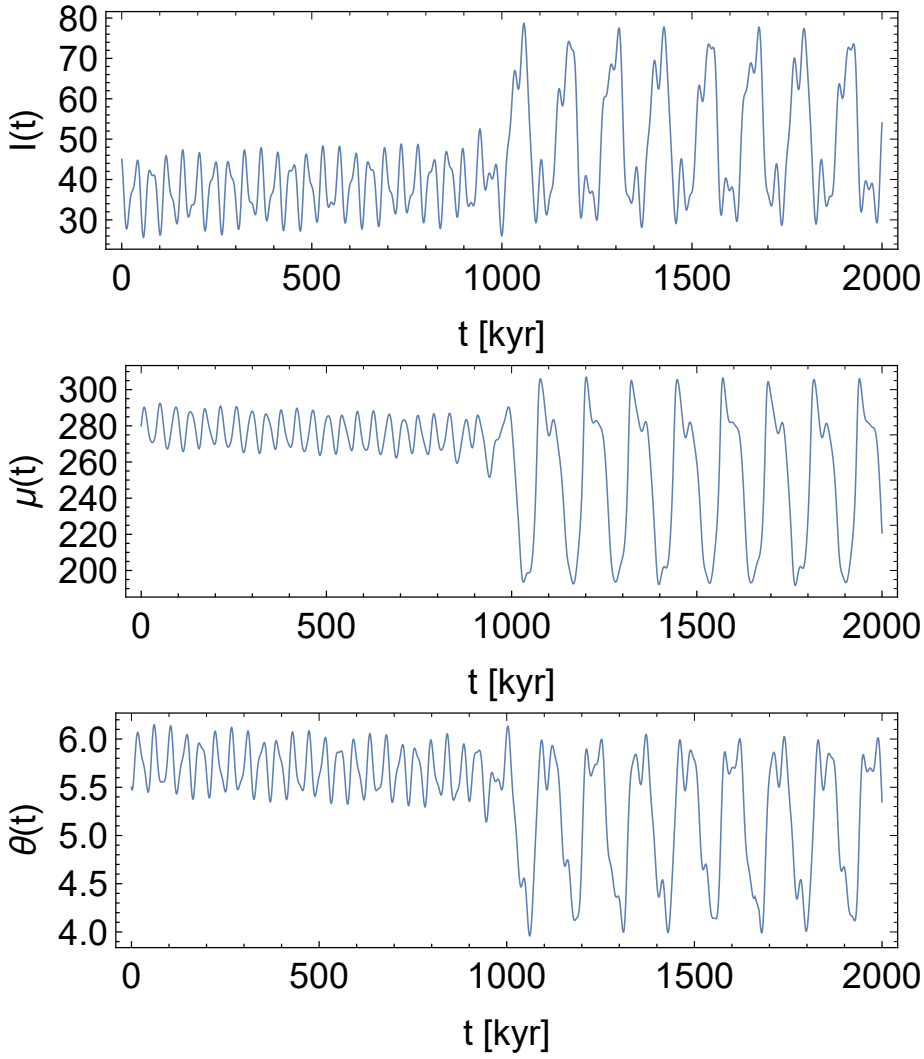

Figure 28: Plots $I(t)$, $\mu(t)$ and $\theta(t)$ with $\beta_1(t)$ as in equation (71) and initial condition $(I, \mu, \theta) = (45, 280, 5.5)$.

We clearly see the change in amplitude and periodicity at 1 Myr, towards larger cycles with a period of around 100 kyr. The position where the Hopf curve is crossed, is chosen such that the period of the cycle matches with this 100 kyr. Note that only a small change in the parameter β_1 is needed to get this MPT behaviour.

3 MPT in the Gildor-Tziperman model

In this chapter, we will study a more involved, physics-based coupled box model of the earth's climate. The model was built for reproducing ice ages oscillations in the late Pleistocene, by Gildor and Tziperman [2, 3, 20]. Whereas the Saltzman-Maasch is a conceptual model of three global averaged variables, this model consists of different coupled boxes (ocean and atmosphere) where the physics of each box is described by their own equations. We start with a simple version of the model [9], and then go on to the 'full model'. A short overview is given of the components of the model, and after that we will simulate the MPT in this model. Note that this is done without a bifurcation analysis; this model is intrinsically time dependent and high dimensional, which makes it virtually impossible to study the bifurcation structure in detail.

3.1 Simple version of Gildor-Tziperman model

To get a feeling of some of the components and equations describing the Gildor-Tziperman model, we first discuss a simple two-variable version of the model. We will give a summary of the important features and repeat some of the results, following the work of Gildor et al. [9]. The model consists of two independent variables, V (land ice volume) and T (temperature). The ice volume is described by the differential equation

$$\frac{dV}{dt} = P(T, a_s) - S(T, t) \tag{73}$$

where P is a function describing the precipitation, depending on temperature, and S a function for the ablation, depending on temperature and time. The precipitation function is given by

$$P(T) = (P_0 + P_1 q(T))(1 - \frac{a_s}{a_o}) \tag{74}$$

where q denotes the amount of water in the atmosphere, a_s is the sea-ice area, a_o the area of the ocean and P_0, P_1 are constants. The sea-ice area is a function of temperature (as a 'switch'), given by

$$a_s(T) = \begin{cases} I_s^0 & \text{if } T \leq T_f \\ 0 & \text{if } T > T_f \end{cases} \tag{75}$$

and for q we have the Clausius-Clapeyron relation

$$q(T) = \frac{q_r \epsilon_q A}{p_s} e^{-B/T} \tag{76}$$

with q_r the relative humidity, p_s the surface pressure and constants ϵ_q, A, B. The function of the ablation is

$$S(T, t) = S_0 + S_M M(t) + S_T(T - 273) \tag{77}$$

with constants S_0, S_M, S_T and $M(t)$ is the normalized deviation of the summer insolation at 65°N from the long term mean. The temperature is described by the differential equation

$$\frac{C_0}{a_0}\frac{dT}{dt} = -\epsilon\sigma T^4 + H_s(1 - \alpha_s\frac{a_s}{a} - \alpha_L\frac{a_L}{a})(1 - \alpha_c). \tag{78}$$

where a_L is the land ice area, C_0 is the heat capacity of the ocean and a is the total area (land and ocean). The constants $\alpha_s, \alpha_L, \alpha_c$ are the values of the albedo of sea-ice, land ice and clouds, respectively. For more information on the model equations and descriptions of the parameters, we refer to [9]. Gildor et al. showed that by a slow variation of the deep ocean temperature, one could simulate the MPT with this simple model. Results are shown in figure 29

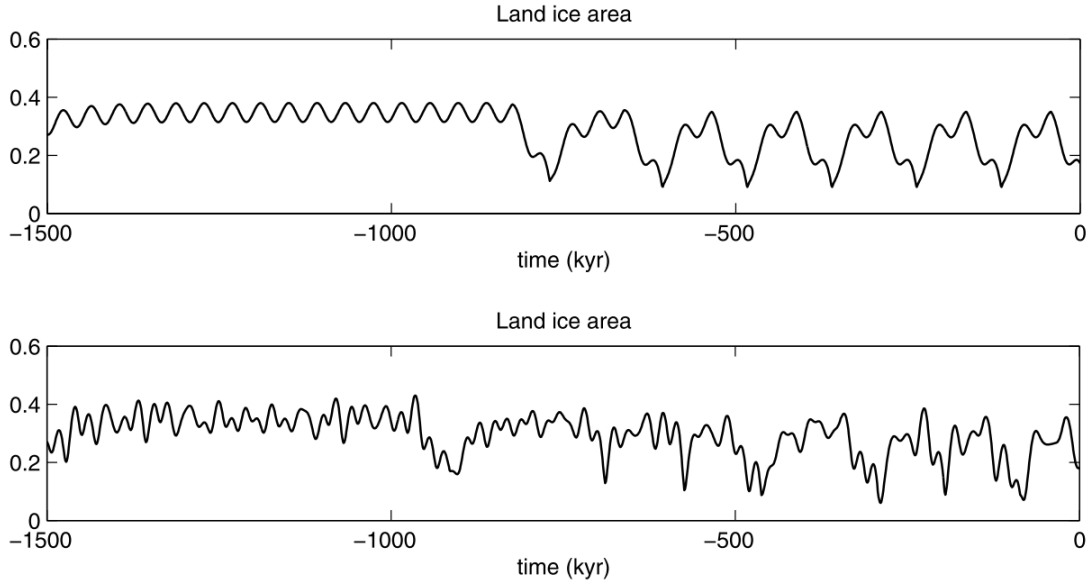

Figure 29: From [9]: Model results for slowly varying deep ocean temperature. Shown is a time series of the fraction of land area covered by land ice. The transition from obliquity and precession (20 and 41 kyr) dominated cycles to 100 kyr ones is seen around -800 kyr. Upper panel: using an idealized insolation curve with a simple periodicity of 41 kyr. Lower panel: using actual Milankovitch summer radiation at 60N.

3.2 Model description of the full model

In this paragraph, we will give a short overview of the full Gildor-Tziperman model. The model consists of different boxes, both atmosphere, land and ocean. Polar ocean boxes can be (partially) covered by sea ice and polar land boxes by land ice. A schematic view of the box-model is given in figure 30. There is also a thermohaline circulation included, this is represented with arrows.

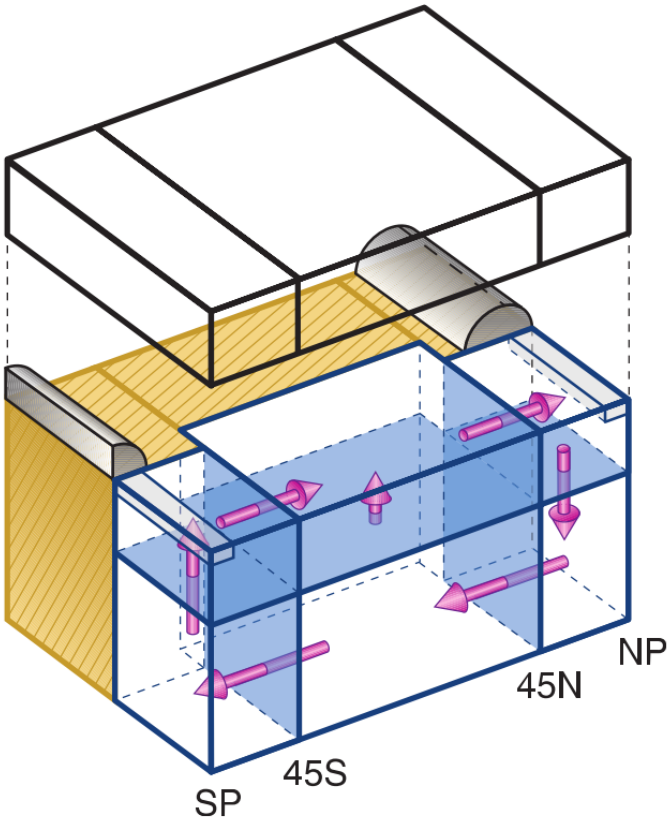

Figure 30: Schematic view of the Gildor-Tziperman model. Figure from [20].

All the physical components of the climate system are allowed to vary and interact, based on the model equations. In the model, it is also possible to include a biogeochemistry module, that also calculates different biological and chemical variables and their interaction. We have not included this module, i.e. we used what Gildor and Tziperman refer to as the 'physics-only' model. However, in order to simulate the MPT more realisticly, we did include a module for the Milankovitch cycles (instead of constant insolation), as you will see in the next paragraph.
We will not repeat the equations of the model here, for that we refer to the code or the literature. Except for the many equations, also the parameter space is very large. We will only mention certain parameters here if we change them with respect to their default

value. Our focus will be on the output of the model. The model is based on forward integration methods and it calculates all important quantities (temperature (atmosphere, ocean), CO_2 concentration, sea/land ice fraction, ...) every 6 hours, for every relevant box. The output consists of 200 year averages (which is more convenient, especially for runs of more than one million years). In the physics-only runs, the CO_2 concentration in the atmosphere has to be prescribed.

As an example, we did a run of 500 kyr with default settings. For the CO_2 concentration, a constant value of 280 ppm (pre-industrial conditions) was prescribed, as can also be seen in the results. In figure 31 we see these default results. We chose to plot the temperature (of the four atmosphere boxes), the sea-ice and land-ice fractions (at both polar boxes) and the CO_2 concentration. In this case, the latter is not very interesting. In general, one can see in that graph which function for the concentration is prescribed.
After a start-up period, we see that the solutions are periodic, with a period of more than 150 kyr. Note that there is always sea ice on the south pole, but this is not the case on the north pole. Sea ice is only formed when the temperature is below a certain threshold, which is the parameter T_{ice}. The default value of this parameter is set on $T_{\text{ice}} = 274$ K. When this value is larger, it is easier to form sea ice. In the land ice signal, we see the characteristic ice age cycles, with slow build-up of ice, and more rapid melt. This asymmetry is also seen in the (indirect) measurements. This is only for the north pole, the land ice fraction at the south pole is held constant in this model.

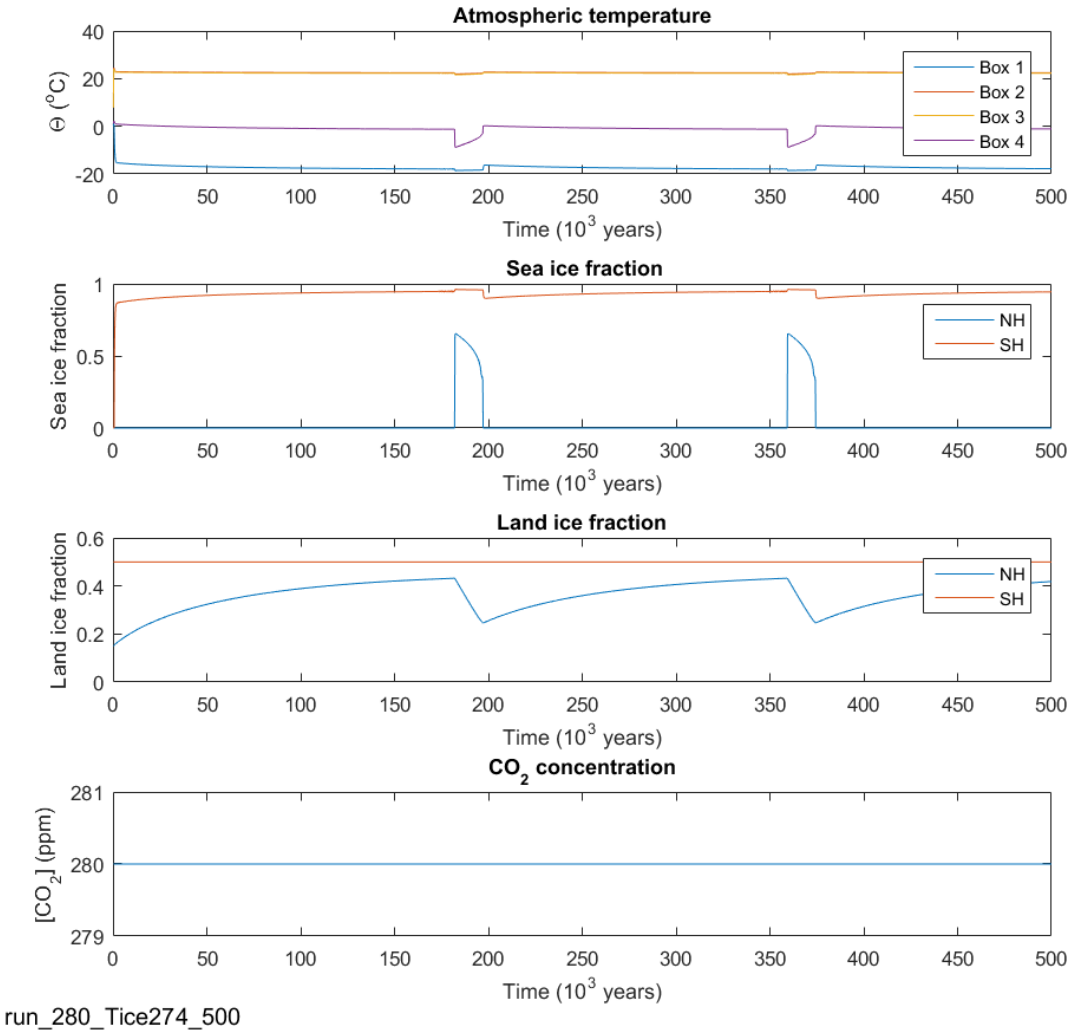

Figure 31: An example solution for constant CO_2 concentration at 280 ppm.

3.3 MPT simulation

In the previous paragraph we have seen that default parameter values and a constant CO_2 concentration of 280 ppm gives oscillations in the solution with a period of approximately 180 kyr. This becomes perhaps more clear when we extend the time to 2 Myr. This is shown in figure 32.

We want to know whether the period of the solution changes, when we change the parameters of the model. In the simple version of the Gildor-Tziperman model, we have seen that a slowly varying deep ocean temperature can trigger an MPT-like transition. To reproduce the same effect in this larger model, we can vary the parameter T_{ice}. The first experiment, is to increase the value from $T_{\text{ice}} = 274$ K to $T_{\text{ice}} = 275.5$ K, i.e. it is again constant. We expect that it will now be easier to form sea ice and therefore the period should decrease. The model run is again over a period of 2 Myr and the results are shown in figure 33. We observe that the period indeed has decreased, to a value of approximately 40 kyr (i.e. the value prior to the MPT).

The next step in our attempt to simulate MPT-like behaviour in the full Gildor-Tziperman model, is to make the parameter T_{ice} time dependent. We start at a value of $T_{\text{ice}} = 275.5$ K and let it decrease by 2.5 K in 2 Myr. By decreasing this threshold, we expect that it gets harder to create sea ice by time. In that sense, the period of the solutions is expected to increase, yielding an MPT-like transition. The results are shown in figure 34.
To make it more realistic, we did the same run also including Milankovitch forcing (by including this module). This results in the graphs of figure 35.
Although we see clearly an increase in the period of the solution in both cases, the transition is rather smooth (not sudden) and the periods are also not exactly 41 and 100 kyr. Therefore, it does not seem to be a bifurcation. It is rather a continuous dependence of the period on the parameter value.

It might not be physically realistic that the T_{ice} parameter has changed in the past. We will now try to find MPT-like behaviour in the model, by a change in the physical quantities. We choose to do this for CO_2, since we have seen so far (in the Saltzman-Maasch model) that CO_2 is a possible trigger for the MPT. In order to investigate this in the Gildor-Tziperman model, we first study the effects of a doubling of the CO_2 concentration, i.e. we increase it to 560 ppm. The new model output is visible in figure 36, for $T_{\text{ice}} = 274$ K.
We see that the period is now approximately 80 kyr, which is smaller than in the default run with a concentration of 280 ppm. However, there are also changes that cannot be explained physically. For example, the average fraction of land ice has increased significantly, which one would certainly not expect when the CO_2 increases. Also the interglacial periods are much shorter than the glacial periods, which is not the behaviour we see in measurements.

Although this model is clearly not physically realistic for large CO_2 concentrations, we can simulate transition behavior by decreasing the CO_2 concentration. We decrease the concentration linearly from 560 ppm to 280 ppm over a period of 2 Myr. This (final) result is shown in figure 37. Note that also the Milankovitch forcing is included again. Also in this figure, we see an increase in the period, however the periods are too large. In general, we see clearly a dependence of the periodicity on the CO_2 concentration. We can simulate MPT-like behavior, but not in a physically feasible way. In that way, the MPT simulation by decreasing T_{ice} is preferred, although it has its own shortcomings.

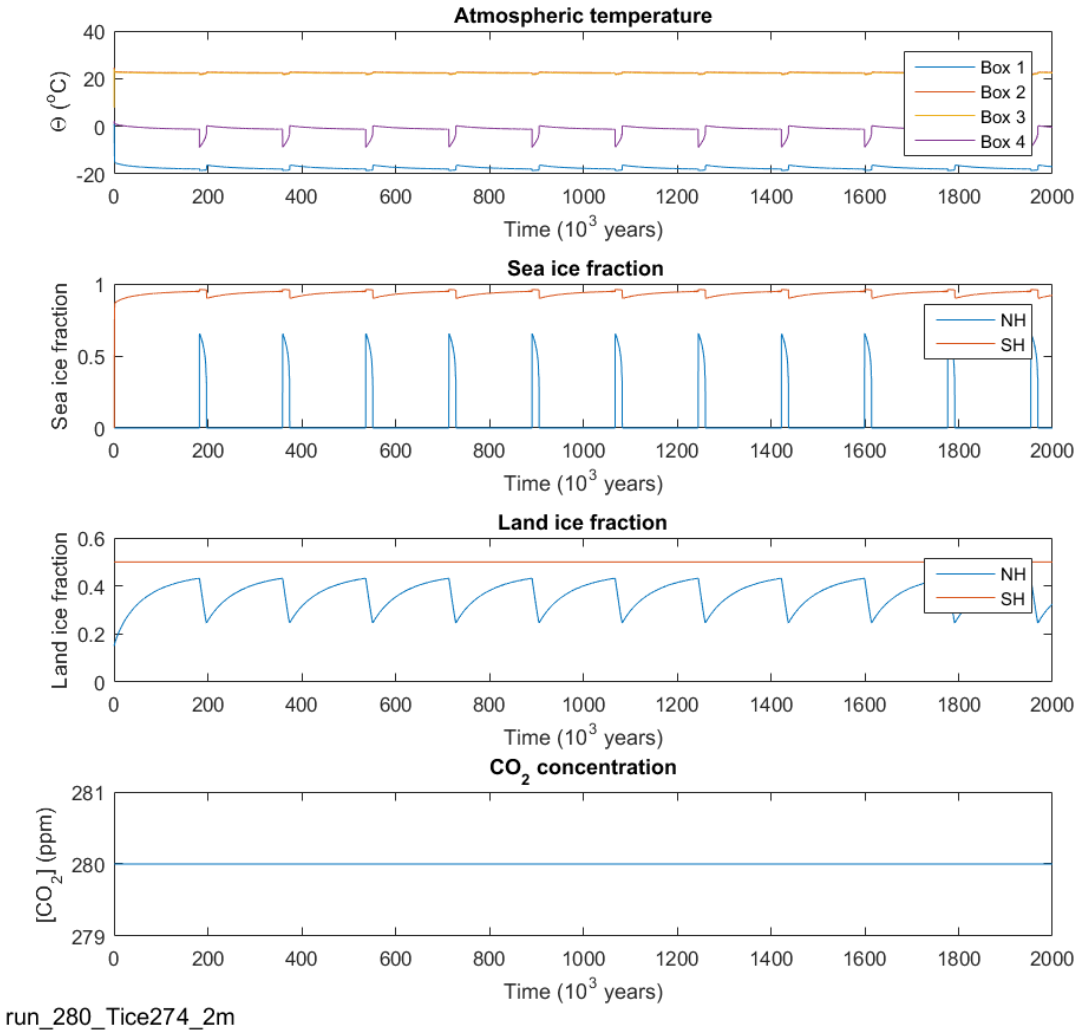

Figure 32: Model solution for constant CO_2 concentration at 280 ppm and $T_{\text{ice}} = 274$ K.

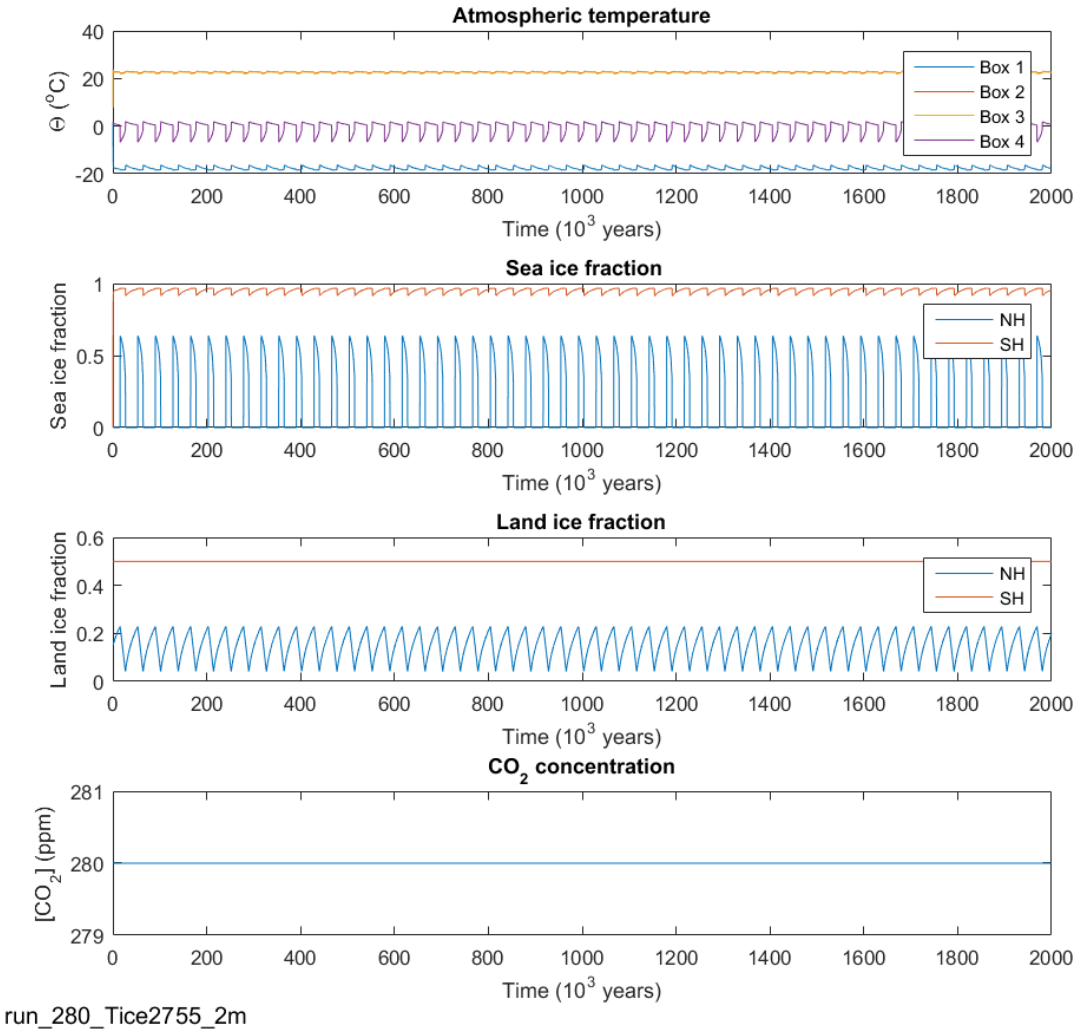

Figure 33: Model solution for constant CO_2 concentration at 280 ppm and $T_{\text{ice}} = 275.5$ K.

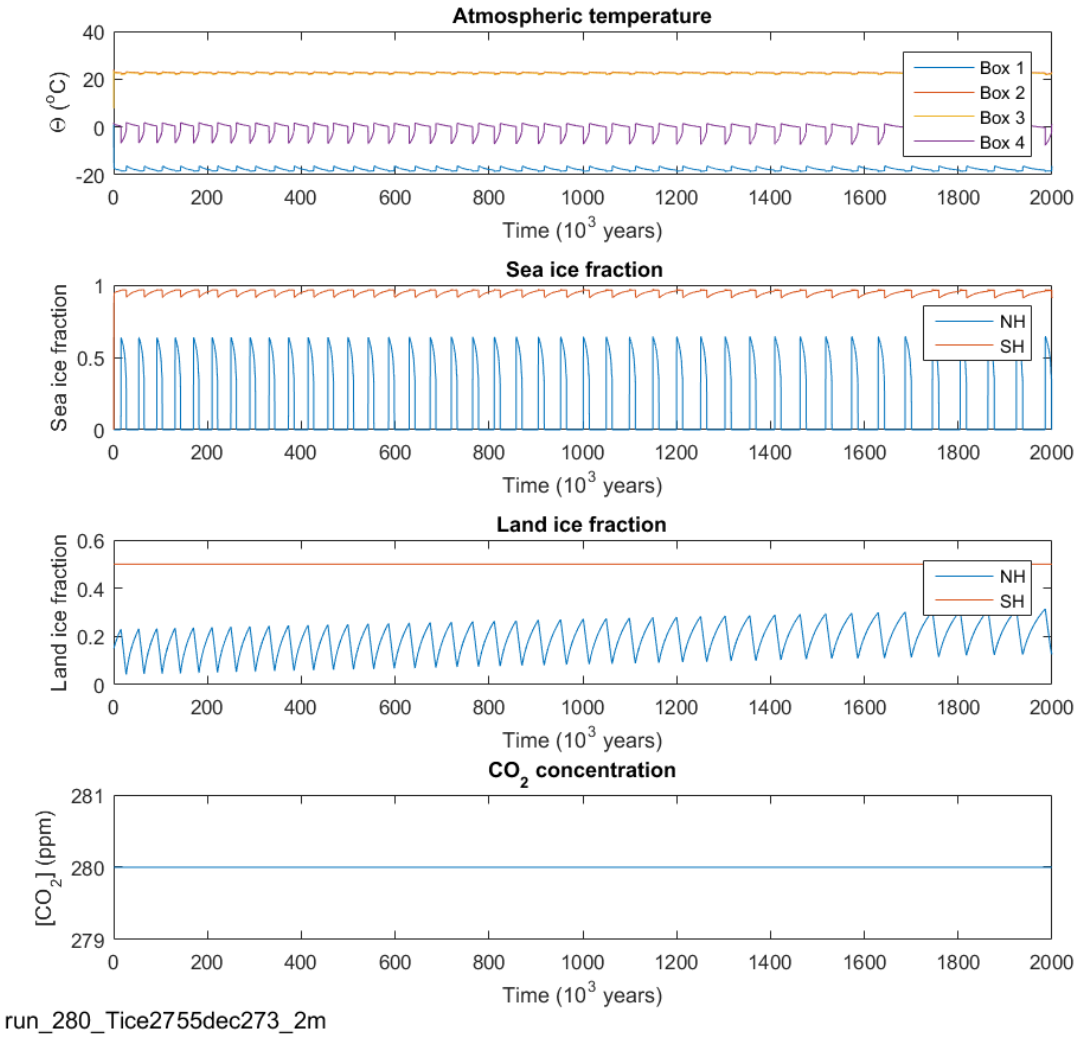

Figure 34: Model solution for constant CO_2 concentration at 280 ppm and a linear decreasing T_{ice}, from 275.5 K to 273 K.

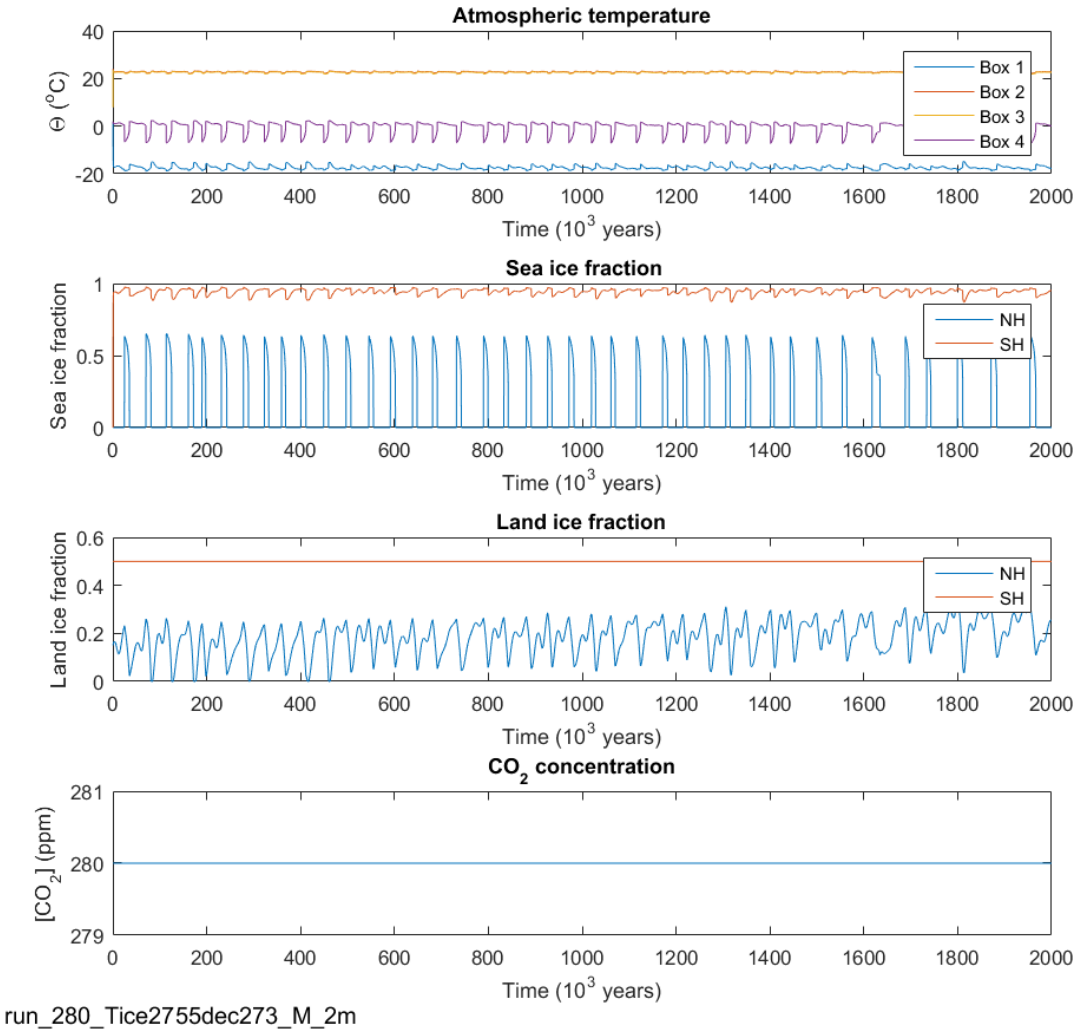

Figure 35: Model solution for constant CO_2 concentration at 280 ppm and a linear decreasing T_{ice}, from 275.5 K to 273 K. Milankovitch forcing is included.

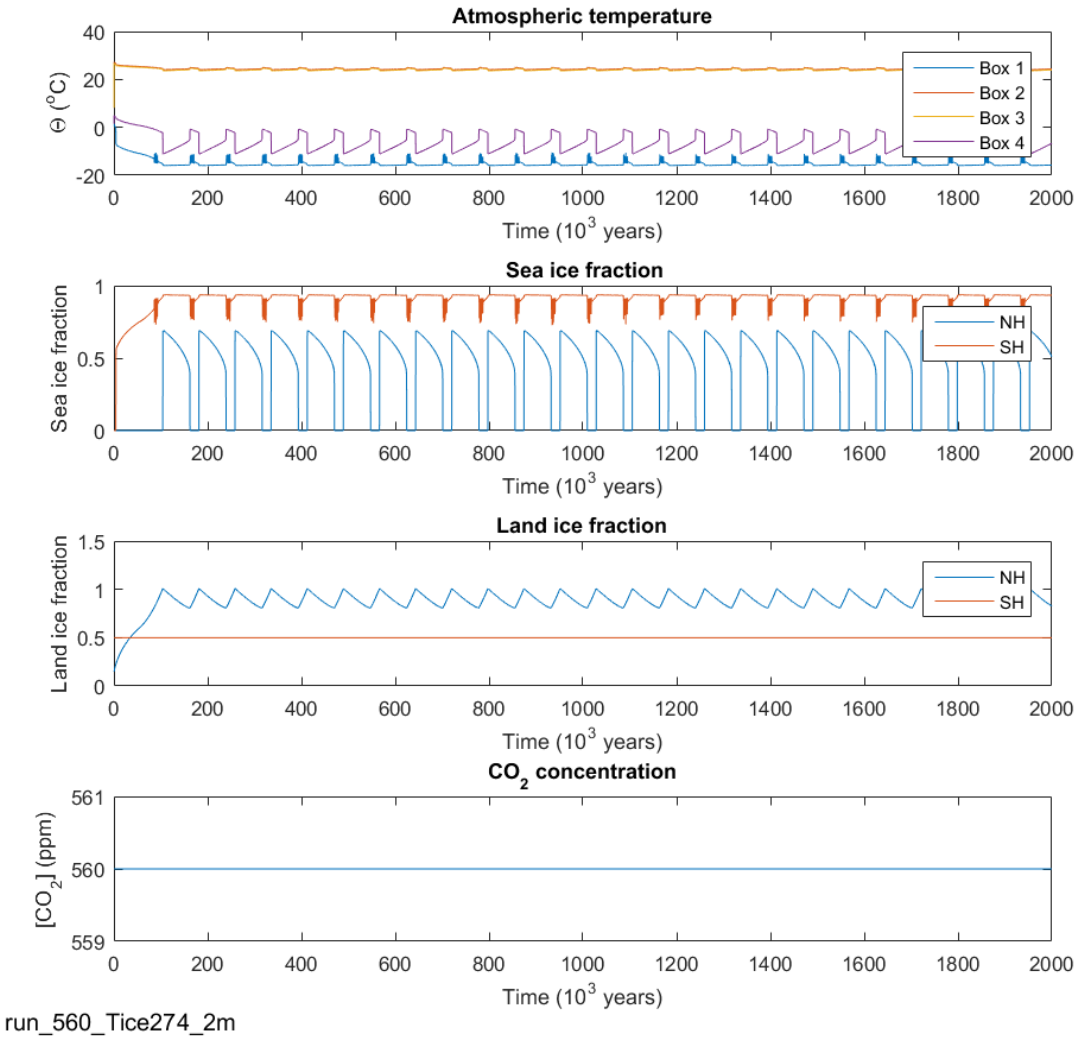

Figure 36: Model solution for constant CO_2 concentration at 560 ppm and $T_{\text{ice}} = 274$ K.

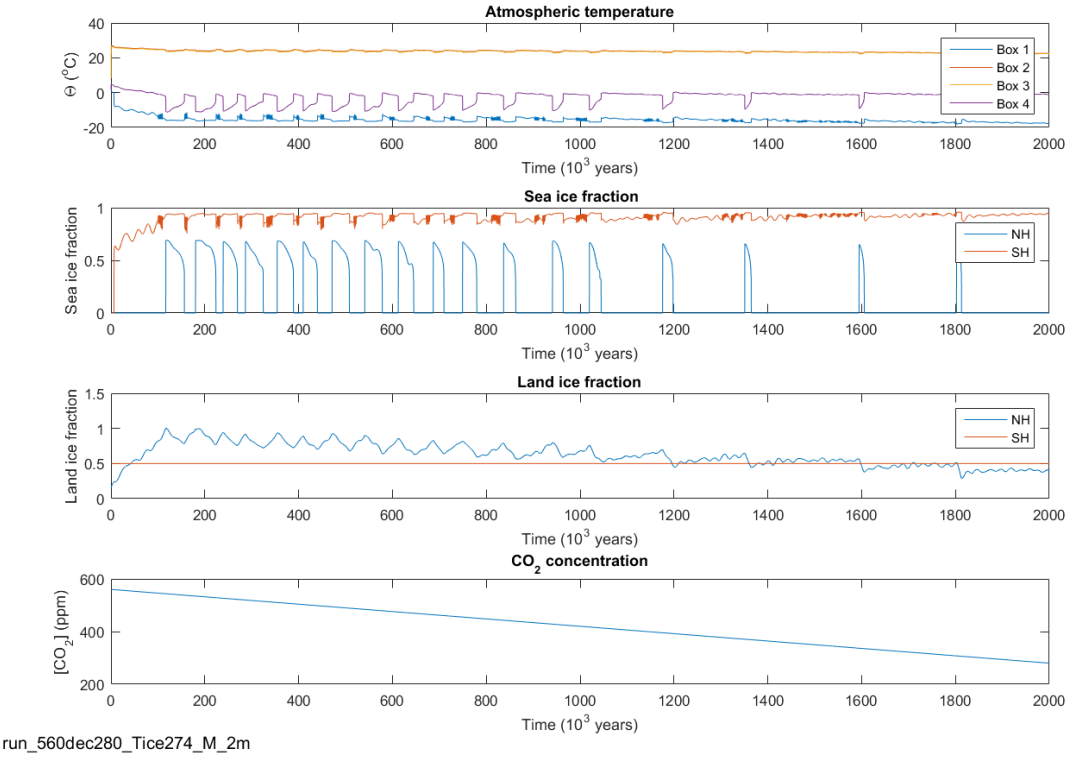

Figure 37: Model solution for a linear decreasing CO_2 concentration from 560 ppm to 280 ppm and constant $T_{\text{ice}} = 274$ K.

Conclusions and discussion

We have (re)introduced the theory of dynamical systems and their bifurcations. We have defined (bifurcation induced) tipping points and via a Hopf bifurcation, we can see the Mid-Pleistocene transition also as a tipping point in the climate system. We have simulated this transition in two (very) different models: a conceptual ODE model of Saltzman and Maasch, and a physics-based box model of Gildor and Tziperman.

In the first case, we could trigger the tipping point by first investigating the bifurcation structure of the model. Crossing the Hopf bifurcation leads to the emergence of a cycle and with Milankovitch-like forcing we could simulate the MPT in both the non-dimensional (2D and 3D) and the full Saltzman-Maasch model.

One should keep in mind that the Saltzman-Maasch model is a conceptual model, also referred to as a 'phenomenological' model. This is because the model equations are based on the phenomenon that you want to describe, and not based on first principles (of physics). However, this very simple model can be analysed thoroughly with the mathematical structure we presented. In that way, we can understand the effects of every parameter change on the solutions of the model. Knowing the bifurcation structure of a model gives a lot of tools to tune the model and find transitional behavior. The results show that a transition like the MPT can be found in this model (in all versions), which matches the data nicely. However, it does not directly give a physical mechanism. We can up to this point only give an explanation for the MPT from a mathematical point of view.

The parameters that we have changed in order to simulate the MPT in the Saltzman-Maasch model, where in the equation of CO_2, both in the non-dimensional cases (2D and 3D) as the full model situation. Although this can of course be a coincidence (the model can be set up this way a priori by Saltzman and Maasch), it at least gives an idea that CO_2 can play an important role in the Mid-Pleistocene transition.

With this in mind, we also were able to simulate MPT-like behavior in the Gildor-Tziperman model. This transition is however not based on knowledge of the bifurcation structure. Although the model is based on physics and therefore also the MPT that is simulated, it also has it flaws. One of them is that the module for land ice is not correct, in the sense that the accumulation (growth) of land ice is not correctly depending on temperature and CO_2. Higher CO_2 leads to more land ice on average, which is counterintuitive. The model has been constructed for very specific research, and is therefore probably only valid in a bounded parameter regime. In other words, the model is not robust for large changes in parameters. The model is, in this form, therefore perhaps not ideal for the purpose of investigating the MPT. Some (maybe rigorous) changes have to be done to the model to make it suitable for future research on this subject.

Another point of criticism might be that it may not be very likely that the parameter T_{ice} is something that has changed the last few million years. From a physics point of view, you would expect that to be (almost) constant, and transitions will most likely be triggered by changes in parameters or variables like the CO_2 concentration. The choice for changing T_{ice} lies in the idea that deep sea changes could have triggered the MPT, and this is one way of simulating this behavior.

There is still future research to be done on the MPT, especially for finding the exact *physical* triggers in the climate system. We have discussed a mathematical theory for these triggers and tested this successfully, but we are still uncertain about the physical mechanism. However, with these results it seems likely that CO_2 has been involved as a possible trigger for the MPT.

References

[1] Barry Saltzman and Kirk A. Maasch. A first-order global model of late Cenozoic climatic change II. Further analysis based on a simplification of CO2 dynamics. *Climate Dynamics*, 5(4):201–210, 1991.

[2] H. Gildor and E. Tziperman. Sea ice as the glacial cycles' climate switch: Role of seasonal and orbital forcing. *Paleoceanography*, 15(6):605–615, 2000.

[3] Hezi Gildor and Eli Tziperman. A sea ice climate switch mechanism for the 100-kyr glacial cycles, 2001.

[4] S. Epstein, R. Buchsbaum, H. A. Lowenstam, and H. C. Urey. Revised Carbonate-Water Isotopic Temperature Scale. *Geological Society of America Bulletin*, 64:1315–1325, 1953.

[5] Johannes Oerlemans. Antarctic ice volume and deep-sea temperature during the last 50 Myr: A model study. *Annals of Glaciology*, 39:13–19, 2004.

[6] Lorraine E. Lisiecki and Maureen E. Raymo. A Pliocene-Pleistocene stack of 57 globally distributed benthic delta 18O records. *Paleoceanography*, 20(1):1–17, 2005.

[7] Rémy J. Petit, D. Raynaud, I. Basile, J. Chappellaz, C. Ritz, M. Delmotte, M. Legrand, C. Lorius, and L Pe. Climate and atmospheric history of the past 420,000 years from the Vostok ice core, Antarctica. *Nature*, 399:429–413, 1999.

[8] Michael Ghil. Cryothermodynamics: the chaotic dynamics of paleoclimate. *Physica D: Nonlinear Phenomena*, 77(1-3):130–159, 1994.

[9] Eli Tziperman and Hezi Gildor. On the mid-Pleistocene transition to 100-kyr glacial cycles and the asymmetry between glaciation and deglaciation times. *Paleoceanography*, 18(1):1–8, 2003.

[10] Peter U. Clark and David Pollard. Origin of the middle Pleistocene transition by ice sheet erosion of regolith. *Paleoceanography*, 13(1):1–9, 1998.

[11] Peter Huybers. Glacial variability over the last two million years: an extended depth-derived agemodel, continuous obliquity pacing, and the Pleistocene progression. *Quaternary Science Reviews*, 26(1-2):37–55, 2007.

[12] Robert Ehrlich. Solar resonant diffusion waves as a driver of terrestrial climate change. *Journal of Atmospheric and Solar-Terrestrial Physics*, 69(7):759–766, 2007.

[13] Gerald E Marsh. Climate Change: The Sun's Role. *Arxiv*, page 16, 2007.

[14] J.J. Duistermaat and W. Eckhaus. *Analyse van gewone differentiaalvergelijkingen*. Epsilon Uitgaven, Utrecht, 4e druk, 2 edition, 2015.

[15] Yuri A. Kuznetsov. *Elements of Applied Bifurcation Theory*. 1998.

[16] A. Dhooge, W. Govaerts, and Yu. A. Kuznetsov. MATCONT: A MATLAB package for numerical bifurcation analysis of ODEs. *ACM Transactions on Mathematical Software*, 29(2):141–164, 2003.

[17] Peter Ashwin, Sebastian Wieczorek, Renato Vitolo, and Peter Cox. Tipping points in open systems: bifurcation, noise-induced and rate-dependent examples in the climate system. *Philosophical transactions of the Royal Society A*, 13:20, 2011.

[18] Kirk A. Maasch and Barry Saltzman. A low-order dynamical model of global climatic variability over the full Pleistocene. *Journal of Geophysical Research*, 95(D2):1955, 1990.

[19] Michel Crucifix. Oscillators and relaxation phenomena in Pleistocene climate theory. *Philosophical Transactions of the Royal Society A: Mathematical, Physical and Engineering Sciences*, 370(1962):1140–1165, 2012.

[20] Hezi Gildor, Eli Tziperman, and J. R. Toggweiler. Sea ice switch mechanism and glacial-interglacial CO2 variations. *Global Biogeochem. Cycles*, 16(3):1032—-, 2002.

[21] Anna S. von der Heydt and Peter Ashwin. State-dependence of climate sensitivity: attractor constraints and palaeoclimate regimes. pages 1–34, 2016.

[22] B. De Boer, R. S.W. Van De Wal, R. Bintanja, L. J. Lourens, and E. Tuenter. Cenozoic global ice-volume and temperature simulations with 1-D ice-sheet models forced by benthic δ18O records. *Annals of Glaciology*, 51(55):23–33, 2010.

[23] Peter Ashwin and Peter Ditlevsen. The middle Pleistocene transition as a generic bifurcation on a slow manifold. *Climate Dynamics*, 45(9-10):2683–2695, 2015.